1-1-1993

Variable structure and singular perturbation control of elastic dynamical systems

Shailaja Chenumalla
University of Nevada, Las Vegas

Order Number 1358560

Variable structure and singular perturbation control of elastic dynamical systems

Chenumalla, Shailaja, M.S.

University of Nevada, Las Vegas, 1994

U·M·I
300 N. Zeeb Rd.
Ann Arbor, MI 48106

VARIABLE STRUCTURE AND SINGULAR PERTURBATION CONTROL OF ELASTIC DYNAMICAL SYSTEMS

by

Shailaja Chenumalla

A thesis submitted in partial fulfillment

of the requirements for the degree of

Master of Science

in

Electrical Engineering

Department of Electrical Engineering

University of Nevada, Las Vegas

May, 1994

The thesis of Shailaja Chenumalla for the degree of Master of Science in Electrical Engineering is approved.

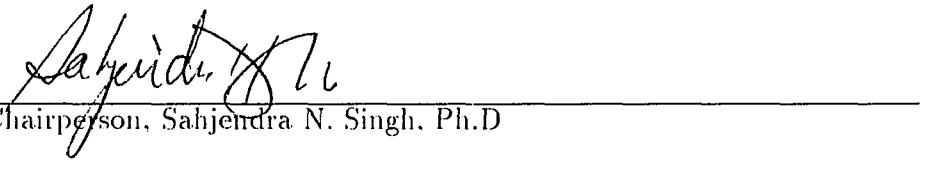

Chairperson, Sahjendra N. Singh, Ph.D

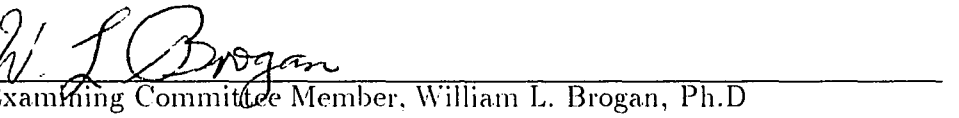

Examining Committee Member, William L. Brogan, Ph.D

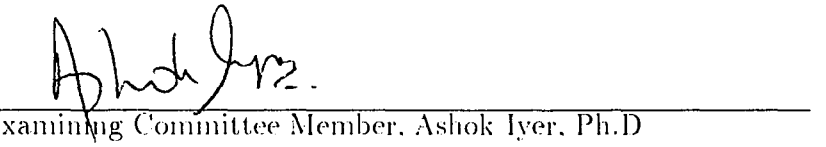

Examining Committee Member, Ashok Iyer, Ph.D

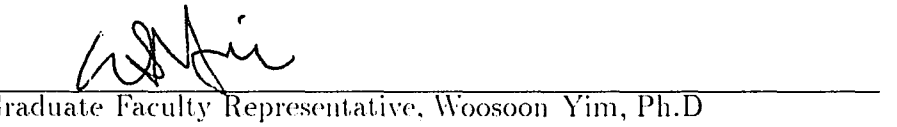

Graduate Faculty Representative, Woosoon Yim, Ph.D

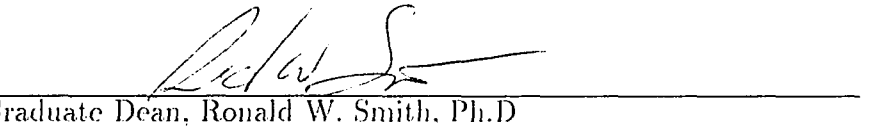

Graduate Dean, Ronald W. Smith, Ph.D

University of Nevada, Las Vegas

May, 1994

ABSTRACT

This thesis treats the question of control of flexible dynamical systems for space applications. Two elastic dynamical systems are considered. The first is an elastic multibody system developed in Phillips Laboratory, Edwards Air Force Base, California. The second systems belongs to the class of elastic spacecraft systems (spacecraft-beam-tip body configuration).

The multibody system developed in Phillips Laboratory, Edwards Air Force Base, CA consists of two elastic links actuated by electric motors at the joints and rotate on a smooth horizontal granite table. An air bearing is used, which allows the whole system to float on the air so that the frictional forces do not exist between the support plate and the granite table. The controlled output is judiciously chosen such that the zero dynamics are stable or almost stable. For the control of the end point, two kinds of parameterizations of end effector position are considered. A variable structure control (VSC) law is derived for the end point trajectory control of each chosen output. Stability of zero dynamics associated with end point control is examined. Although, the VSC law accomplishes precise end point tracking, elastic modes are excited during the maneuver of the arm. A linear stabilizer is designed for the final capture of the terminal state.

The second flexible system considered in this thesis is the elastic space vehicle. For the attitude control and vibration stabilization of the elastic space craft (spacecraft-beam-tip body configuration), Singular Perturbation technique is used. Based on nonlinear inversion, a control law is derived to decouple the attitude angle and the dominant flexible modes from the remaining elastic modes. The inverse control law decomposes the spacecraft dynamics into a slow and a fast subsystem. Based on singular perturbation theory, controllers are designed for each lower-order subsystem. Then a composite state feedback control is obtained by combining the slow and the fast control laws.

Simulation results are presented in both cases to show that the control system accomplishes the trajectory tracking and vibration damping in the closed-loop system.

Contents

ACKNOWLEDGMENTS

At the outset, I would like to thank Dr. Sahjendra N.Singh, for all his painstaking efforts and the help he has extended to me during the course of my graduate program. But for his constant encouragement and thoughtful guidance, completion of this thesis would have been beyond my capability. I extend my sincere gratitude to Dr. William L. Brogan for his invaluable help. I would like to thank Dr. Ashok Iyer for all his help and advise during various phases of my graduate study at UNLV. Special thanks are due to Dr. Woosoon Yim, for agreeing to be on my thesis committee. I would also like to thank Dr. Yahia Baghzouz, Chairman, and Doreen Martinez, Secretary, of Electrical Engineering Department for all their help extended to me during my graduate study here. And last, but not the least, I would like to thank Dr. Alok Das (PL/Edwards AFB) for his suggestions and constant support and Mr. Monty Smith (PL/Edwards AFB) for the valuable discussions related to the multibody laboratory experiment. With love and affection I dedicate this humble effort to my parents Mr. Lakshman Rao and Mrs. Sharada. Finally I thank God for making all this happen.

Chapter 1

INTRODUCTION

Design of flexible dynamical systems is of current interest of many researchers. Such dynamical systems are energy efficient. The control of this class of systems is complicated because of the interaction of rigid and flexible modes.

The two systems considered in this thesis belong to the class of flexible systems. The first is the elastic multibody system developed in Phillips Laboratory, Edwards Air Force Base, CA. This system consists of two elastic links and two revolute joints. The second system considered is the flexible spacecraft (orbiter)-beam-tip body (antenna or a reflector) configuration. Both these systems are used in space applications. The structure of the mathematical model of these two systems is some what similar. The nonlinearity and large dimension due to the presence of flexible modes in these systems create difficulty in the design of the control law.

In the Phillips Laboratory, Edwards Air Force Base, CA, a multibody system has been

set up for the study of dynamics and control-structure interaction. This project is called the Planar Articulating Controls Experiment (PACE). The system has two elastic links and two revolute joints. The arm rotates in the horizontal plane on a smooth granite table. An air bearing is used, which allows the whole system to float on air so that the friction forces do not exist between the support plate and the granite table. When the arm is maneuvered, both the links undergo elastic deformation. The design of controllers for the systems belonging to this class is complicated because of the nonlinearity in the equations of motion and the presence of uncertainty in the system.

Recently some theoretical and experimental related to end point control have been done [1-11]. In these papers, inverse control systems [1-4, 8-10] and variable structure systems [11,12,13] have been designed. Variable structure control system is relatively insensitive to large parameter variations, but the control law is a discontinuous function of the state variables. The variable structure controller design of Ref.11 considers parameterized output vector of end points of each link. However, it is desirable to design controller so that the end effector of the multibody system can be directly controlled.

This research is related to end point trajectory control of the multibody system. For the trajectory control, a control law based on variable structure system (VSC) theory [12,13] is derived. It turns out that the zero dynamics corresponding to the endpoint control in the closed-loop system is unstable [11]. Instability of the zero dynamics is avoided by choosing the coordinates of a point in the neighborhood of the tip position of controlled output variables. Such a choice of controlled outputs is not unique. We have made two parame-

terizations of the controlled output in this study. The first parameterization of the output vector defines the angular position of the end effector directly and thus differs from that of Ref.11. However, the second parameterization which is similar to Ref.11 is also treated for comparison. Each parameterization of the output leads to a different control law for the trajectory control. Using the VSC law, tip trajectory is accurately tracked. However, this excites the elastic modes of the links. Based on a linearized system about the terminal equilibrium point, a stabilizer is designed using pole assignment technique. Simulation results are presented to show that in the closed-loop system, precise trajectory tracking and vibration damping are accomplished in spite of payload uncertainty.

The second system considered in this thesis (i.e the elastic spacecraft) belongs to the class of large, flexible space vehicles. An important class of shuttle deployed payloads consists of cantilevered beam-like structures with massive tip bodies. Presently, there is considerable interest in the problem of stability and control of such flexible space vehicles. Large angle rotational maneuver of spacecraft induces structural deformation in the flexible appendages. Dynamical models of space vehicles are nonlinear and include the rigid and flexible mode interaction. The large dimension and nonlinearity in the system create difficulty in the design of control systems for rotational maneuver of spacecraft.

In the recent years, several studies related to control of flexible space vehicles have been done and linear and nonlinear control systems have been designed [18-32]. An excellent survey of research in this area has been published in [33] which provides a good source of references. Optimal controller for flexible spacecraft has been designed in [18]. Time optimal

slewing of linear and nonlinear flexible spacecraft has been treated in [19,20], and bang-bang rest-to-rest maneuver of linear models has been considered in [21,22]. Near-minimum time single axis slewing of flexible vehicle has been treated in [23,24]. A perturbation method has been used to obtain a feedback controller in [25]. Lyapunov stability theory has been used to design controllers for the maneuver and vibration control of space vehicles in [26,27]. Controllers based on inversion [16] and feedback stabilization have been derived [28,29] and adaptive control of flexible spacecraft has also been considered [30]. Sliding mode control theory has been used in [31,32] to derive robust discontinuous controllers for the control of flexible vehicles.

In these papers, controller design is based on the complete large order model of the space vehicle. It is well known that the dynamics of flexible systems such as elastic space vehicles and light-weight robotic manipulators include the interaction of the slow rigid modes and the high frequency, fast elastic modes. The presence of slow and fast variables in the system's dynamics leads to numerically ill-conditioned control problems. Such systems belong to the class of singularly perturbed systems for which singular perturbation control theory [34-37] gives elegant synthesis techniques for controller design. An interesting feature of singular perturbation technique is that it decomposes the original design problem into a slow subproblem and a fast subproblem related to a reduced order slow subsystem and a lower order fast boundary layer subsystem, respectively for which the design is done relatively easily. Recently, a singular perturbation technique has been used for the control of elastic robots [38,39]. Since flexible space vehicles include slow and fast state variables, it will be of interest to explore the applicability of the singular perturbation methodology for

the design of the controllers for the attitude control.

In this thesis, we consider rotational maneuver of an elastic spacecraft (orbiter-team-tip body configuration) shown in Fig.2. Although, the approach of this paper is applicable to three axis maneuvers, for simplicity, only single axis control of the pitch angle is considered. The spacecraft is controlled by a torquer on the orbiter and a torquer and a force actuator on the tip body. When the spacecraft is maneuvered, the beam connecting the orbiter and the end body experiences structural deformation. The problem of interest here is to control the orientation and to damp the transverse vibration of the beam.

For the derivation of control system for large pitch angle rotational maneuver and vibration suppression of the spacecraft nonlinear inversion and singular perturbation technique is used, An inverse control law was derived to decompose the spacecraft dynamics into a slow subsystem and a fast subsystem. Based on singular perturbation theory, controllers are designed for each lower-order subsystem. The derivation of the complete control system is in the spirit of [39] where a similar approach has been used for controlling elastic robotic arm. Simulation results are presented to show that the composite control system accomplishes large angle rotational maneuver and vibration suppression in the closed loop system.

The organization of this thesis is as follows: The mathematical model of the two flexible dynamical systems is presented in Section 2. Section 3 presents the Variable Structure Control scheme for the end point control of the elastic multibody system. Section 4 presents a brief introduction to the Singular perturbation technique and a composite control law is

derived. Section 5 presents the control of elastic spacecraft by nonlinear inversion and singular perturbation and Section 6 presents the conclusions.

Chapter 2

MATHEMATICAL MODEL AND THE CONTROL PROBLEM

In this chapter the mathematical models of the two elastic systems considered in this thesis. In the first section the mathematical model of the elastic multibody system developed in Phillips Laboratory, Edwards Air Force Base. CA is described and the second chapter presents the mathematical model of the elastic spacecraft.

2.1 Mathematical Model Of the Elastic Multibody

Fig. 1 illustrates the elastic multibody system with two elastic links. Both the joints are revolute and torque is applied at these joints by actuators. In this design it is assumed that the gravity is zero, which is valid as the elastic manipulator is developed for space applications. Also, it is assumed that the base is fixed and the design does not include the dynamics of the space vehicle. This assumption is valid for those applications in which the space vehicles are large compared to the elastic manipulator.

In the Fig.1 OXY is an inertial frame with origin at joint 1, OX_1Y_1 is a reference frame with X_1 along link 1, and OX_2Y_2 is a reference frame with origin at joint 2 with X_2 axis along link 2. OX_1 and O_2X_2 are tangent to the links. $OO_{N1}O_{N2}$ represents the position of the arm for the case of rigid links. θ_1 and θ_2 are the joint angles when rigid conditions are assumed. OO_2O_{E2} represents the position of the deformed arm.

By the assumed mode method, any arbitrary solution of flexible motions can be assumed to be composed of a linear combination of admissible functions multiplied by time-dependent generalized coordinates. Let $\delta_1(l_1,t)$ and $\delta_2(l_2,t)$ denote the elastic deflections of the links at a distance l_1 from O along OX_1 and at a distance l_2 from O_2 along O_2X_2. Also, $\phi_{1j}(l_1)$, $\phi_{2j}(l_2)$ are the necessary admissible functions for clamped-free beams. In this study, ϕ_{ij} are assumed to be the mode shapes of a clamped-free beam.

Let $q_{1i}(t)$ and $q_{2i}(t)$ be the generalized coordinates. The flexible displacements of the two links can be expressed as

$$\begin{aligned} \delta_1(l_1,t) &= \sum_{i=1}^{n} \phi_{1i}(l_1) q_{1i}(t) \\ \delta_2(l_2,t) &= \sum_{i=1}^{n} \phi_{2i}(l_2) q_{2i}(t) \end{aligned} \tag{2.1}$$

where n denotes the number of significant modes. Here it is assumed that the links do not undergo longitudinal and torsional deformations and the contribution of higher modes is negligible.

The equations of motion of the arm can be obtained by Lagrangian method. These are

given by

$$\frac{d}{dt}(\frac{\partial T}{\partial \dot{z}_i}) - \frac{\partial T}{\partial z_i} + \frac{\partial P}{\partial z_i} = B_1 u \tag{2.2}$$

where

$z = (\theta^T, q^T)$, $\theta = (\theta_1, \theta_2)^T$, $q = (q_{11}, \cdots, q_{1n}, q_{21}, \cdots, q_{2n})^T$,

T is the kinetic energy of the arm,

P is the potential energy of the arm,

$u = (u_1, u_2)^T$,is the vector of joint torques,

$B_1 = [I_{2\times 2}, O_{2\times 2n}]^T$

Here, T denotes transposition and I and O denote the identity and null matrices of indicated dimensions.

The kinetic energy for each link is a quadratic function of generalized velocities and is given by $T = (\dot{z}^T M(z)\dot{z}/2)$ where $M(z)$ is the positive definite symmetric inertia matrix and is a nonlinear function of z. Using this expression of T in (2.2), gives (see [17] for the complete derivation)

$$M(z)\ddot{z} + h_o(z, \dot{z}) + \partial P(z)/\partial z = B_1 u \tag{2.3}$$

where

$h_o(z, \dot{z}) = \dot{M}(z)\dot{z} - (1/2)(\partial \dot{z}^T M(z) - z/\partial z)$

$$M(z) = \begin{bmatrix} M_{11}(z) & M_{12}(z) \\ M_{21}(z) & M_{22}(z) \end{bmatrix}$$

where M_{11} is a 2×2 submatrix.

Defining $x = (z^T, \dot{z}^T)^T$, one obtains a state variable representation of (2.3) given by

$$\dot{x} = f(x) + B(x)u \tag{2.4}$$

where

$$n_0 = 2(n+1),$$

$$f(x) = \begin{bmatrix} \dot{z} \\ M^{-1}(z)(-h_0(z,\dot{z}) - \partial P(z)/\partial z) \end{bmatrix} \triangleq \begin{bmatrix} \dot{z} \\ h(z,\dot{z}) \end{bmatrix}$$

$$B(x) = \begin{bmatrix} O_{2\times n_0}, & (M^{-1}(z)B_1)^T \end{bmatrix}^T$$

$$h(z,\dot{z}) = -h_0(z,\dot{z}) - \partial P(z)/\partial z$$

To this end a judicious choice of the controlled variables is made for the design of the control system. Assuming small elastic deflections, the angular positions of the links are given by

$$\rho_{it} = tan^{-1}\left[\frac{sin(\theta_i + \frac{\delta_i(L_i,t)}{L_i})}{cos(\theta_i + \frac{\delta_i(L_i,t)}{L_i})}\right], i = 1,2$$

$$\rho_{et} = tan^{-1}\left[\frac{L_1 sin(\theta_1 + \frac{\delta_1(L_1,t)}{L_1}) + L_2 sin(\theta_1 + \theta_2 + \frac{\delta_2(L_2,t)}{L_2})}{L_1 cos(\theta_1 + \frac{\delta_1(L_1,t)}{L_1}) + L_2 cos(\theta_1 + \theta_2 + \frac{\delta_2(L_2,t)}{L_2})}\right] \tag{2.5}$$

Here ρ_{1t}, and ρ_{2t} are the angular positions of the end points of the link 1 and link 2, respectively, but ρ_{et} is the angular position of the end effector of the arm (see Fig.1). Thus, for $i = 1,2$, one has from (2.5) that

$$\rho_{it} = \theta_i + \frac{\delta_i(L_i, t)}{L} \tag{2.6}$$

where $L_i (i = 1, 2)$ denote the lengths of the links.

Although, one can consider ρ_{et} given in (2.5) for the controller design, certain simplification results for the arm model developed in the Phillips Laboratory for which $L_1 = L_2$. Using $L_1 = L_2 = L$ in (5) and simplifying, gives

$$\rho_{et} = \theta_1 + \frac{\theta_2}{2} + \frac{1}{2}\left(\frac{\delta_1(L, t) + \delta_2(L, t)}{L}\right) \tag{2.7}$$

According to (2.6) and (2.7) ρ_{it} and ρ_{et} denote the angular position of the end points of the links and the end effector. One can choose these as output variables for control system design. However, it will be seen later that such a choice leads to unstable zero dynamics. In order to avoid instability of the zero dynamics, we shall choose angular positions of points close to the end points of the links as output variables. These are given by either of the two sets of output vectors OV_1, and OV_2 defined as

$$y = \begin{bmatrix} \rho_1 \\ \rho_e \end{bmatrix} = \begin{bmatrix} \theta_1 + \alpha_1 \frac{\delta_1(L_1, t)}{L_1} \\ \theta_1 + \frac{\theta_2}{2} + \frac{1}{2}\left(\frac{\alpha_1\delta_1(L,t) + \alpha_2\delta_2(L,t)}{L}\right) \end{bmatrix} \qquad (OV_1) \tag{2.8}$$

$$y = \begin{bmatrix} \rho_1 \\ \rho_2 \end{bmatrix} = \begin{bmatrix} \theta_1 + \alpha_1 \frac{\delta_1(L_1, t)}{L_1} \\ \theta_2 + \alpha_2 \frac{\delta_2(L_2, t)}{L_2} \end{bmatrix} \qquad (OV_2) \tag{2.9}$$

We have chosen OV_1 and OV_2 as two forms of parameterized output variables where the parameter $\alpha_i \in [0,1]$. For $\alpha_i = 1, i = 1,2$, one obtains the angular positions of the tip of the links and $\alpha_i = 0$ corresponds to the angular position of the links if the arm is rigid. For $\alpha_i \in [0,1)$, outputs are the angular positions of points close to the end points of the links. The choice of the outputs in (2.8) and (2.9) leads to different control laws. We notice that the parameterization (OV_1) includes the position of a point close to the end effector position, and it is useful in the practical implementation since the neighboring end effector trajectory error can be directly fed back in a natural way for fine position control. However, the control system designed based on the output vector (OV_1) is relatively complicated.

Let $y_r(t) = [y_{r1}(t), y_{r2}(t)]^T$ be a given reference trajectory. We are interested in designing control system such that in the closed-loop system $y(t)$ tracks $y_r(t)$ and elastic vibration is suppressed.

2.2 Mathematical Model Of the Elastic Spacecraft

Fig.2 shows the elastic spacecraft. Here only the maneuver in the pitch plane is considered. A right-handed coordinate frame (denoted as S_0) with axes X_0, Y_0, Z_0 is fixed to the spacecraft with its origin at the mass center of the spacecraft. X_I, Y_I, Z_I are the axes of an inertial frame S_I. The coordinate system S_1 with axes X_1, Y_1, Z_1 is obtained by the translation of the frame S_0 at the attachment point of the beam and the orbiter. The attitude of the spacecraft is given by the pitch angle θ which is the angle of rotation of the spacecraft about the axis Z_0. When the spacecraft is slewed about the Z_0 axis, the beam is allowed to undergo elastic transverse bending in the $Y_0 - Y_0$ plane. The attachment

point O of the beam and orbiter is located arbitrarily with respect to the mass center of the spacecraft, but it is assumed that the mass center of the tip body is located along the tangent line to the beam at the tip point.

Beginning with a hybrid set of partial differential and ordinary differential equations describing the elastic deformation of the beam and the rotational motion of the spacecraft, Storch and Gates[40] have obtained a complete derivation of the equations of motion of this spacecraft in a rigorous way. The equations of motion are given by

$$
\begin{aligned}
& a_{00}\ddot{\theta} + \sum_{k=1}^{m} a_{1k}\ddot{p}_k = [\ b_{01}\ \ b_{01}\ \ b_{03}\ ]u \\
& a_{1i}\ddot{\theta} + \sum_{k=1}^{m} (\delta_{ik} - \frac{\rho L}{m} u_{3i}u_{3k})\ddot{p}_k = [\ 0\ \ b_{i2}\ \ b_{i3}\ ]u + u_{3i}\mu_0 a_2 \frac{\dot{\theta}^2}{L} - \Omega_i{}^2 p_i \qquad (2.10) \\
& \qquad\qquad\qquad\qquad\qquad\qquad\qquad\qquad\qquad\qquad (i = 1, 2, \cdots, m)
\end{aligned}
$$

where the control vector $u = (u_1, u_2, u_3)^T = (T_s, T_p, F)^T \in R^3$ (T denotes transposition); T_s is the external control moment applied to the orbiter; T_p and F are the control moment and force applied on the tip body at its mass center along axes parallel to Z_1 and Y_1, respectively, and p_i denotes the ith elastic mode. In this model, a finite number of elastic modes have been retained assuming that the first m modes are significant and adequately approximate the elastic deformation of the beam. The parameters $a_{ij}, b_{ij}, u_{ij}, \Omega_i$, etc are given in the appendix for completeness. The system is nonlinear due to the presence of the $(\dot{\theta}^2)$ term in the model. The transverse elastic deformation δ_e along the axis Y_1 at any point at a distance l from the attachment point O of the spacecraft and the beam is given by

$$\delta_e(l,t) = L\sum_{k=1}^{m} p_k(t)\beta_k(\eta), \quad \eta = \frac{l}{L} \tag{2.11}$$

where $\beta(\eta)$ is the kth mode shape, and L denotes the length of the beam.

The set of equations (2.10) can be written in the compact form as

$$\begin{pmatrix} D_{11} & D_{12} \\ D_{12}^T & D_{22} \end{pmatrix} \begin{bmatrix} \ddot{\theta} \\ \ddot{p} \end{bmatrix} = \begin{bmatrix} 0 \\ g \end{bmatrix} \dot{\theta}^2 - \begin{bmatrix} 0 \\ K \end{bmatrix} p + B_0 u \tag{2.12}$$

where, $p = (p_1, \cdots, p_m) \in R^m$ and the positive definite symmetric inertia matrix is $D \triangleq (D_{ij}), i, j = 1, 2$. Here the matrix B_0 can be obtained by equating similar terms in (2.10) and (2.12), and

$$\text{K=diag}(\ \Omega_i{}^2), i = 1, \cdots, m$$

$$\text{g=}(\mu_0 a_2/L)(u_{31}, \cdots, u_{3m})^T$$

Define $H \triangleq D^{-1}$, and $z = (\theta, p^T)^T \in R^{(m+1)}$. Then solving (2.12), gives

$$\ddot{z} = H_1 g\dot{\theta}^2 + H_2 K p + H B_0 u \tag{2.13}$$

where $H = [H_1, H_2]$, and H_1 denotes the first column of H.

Suppose that a third order reference model

$$\dddot{\theta}_r + 3\lambda_c \ddot{\theta}_r + 3\lambda_c{}^2 \dot{\theta}_r + \lambda_c{}^3 \theta_r^* = 0 \tag{2.14}$$

is given where $\lambda_c > 0$ and θ^* is the determined value of the pitch angle. The characteristic polynomial of (2.14) is

$$(\lambda + \lambda_c)^3 = 0 \tag{2.15}$$

Since $\lambda_c > 0$, the system (2.14) is asymptotically stable.

We are interested in deriving a control system such that in the closed-loop system, the attitude angle $\theta(t)$ tracks the reference trajectory $\theta_r(t)$, and the elastic oscillations are damped out. For a proper choice of reference trajectory, the spacecraft attains the desired orientation, as $\theta(t)$ converges to $\theta_r(t)$.

Chapter 3

SLIDING MODE CONTROL SCHEME

3.1 Introduction

This chapter presents the Variable Structure control scheme and Elastic mode stabilization for the trajectory control of the elastic multibody system developed in Phillips Laboratory, Edwards Air Force Base, California. Simulation results are presented to show that precise trajectory tracking and vibration damping are accomplished in spite of payload uncertainty

For the end point control of the multibody system, a control law based on Variable Structure Systems theory is developed. The sliding controller provides a systematic approach to the problem of maintaining stability and consistent performance for the class of systems to which it applies. It is relatively insensitive to large parameter variations. Variable Structure System Theory involves the choice of a switching surface in the state space

which is commonly called as sliding surface. A discontinuous control law is derived which switches when the desired output trajectories cross this hypersurface.

The motion of the system trajectories consists of two stages: the reaching mode and the sliding mode. The phase of operation when the system trajectory is attracted towards the defined switching surface from any initial condition constitutes the reaching phase. Once on the switching surface, the system trajectories are confined to this surface and any subsequent motion of the trajectories involves the sliding of the trajectories on this surface. This phase is called the sliding mode.

The function defining the sliding surface includes the integral of the output trajectory error. This is useful to improve the performance of the system. The discontinuous control law accomplishes precise end point tracking of the desired output trajectory. However, this excites the elastic modes of the links. Based on a linearized system about the terminal equilibrium point, a stabilizer is designed using pole assignment technique.

In the following sections the Robot arm control problem is defined and the design of Variable Structure Controller and the linear stabilizer is presented.

3.2 Robot Arm Control Problem

From Chapter 2, using Lagrangian method, the equations of motion have been given.

From (2.2) one obtains

$$M(z)\ddot{z} + h_o(z,\dot{z}) + \partial P(z)/\partial z = B_1 u \tag{3.1}$$

where

$h_o(z,\dot{z}) = \dot{M}(z)\dot{z} - (1/2)(\partial \dot{z}^T M(z)\dot{z}/\partial z)$

$$M(z) = \begin{bmatrix} M_{11}(z) & M_{12}(z) \\ M_{21}(z) & M_{22}(z) \end{bmatrix}$$

where M_{11} is a 2×2 submatrix.

Defining $x = (z^T, \dot{z}^T)^T$, one obtains a state variable representation of (3.1) given by

$$\dot{x} = f(x) + B(x)u \tag{3.2}$$

where

$n_0 = 2(n+1)$,

$$f(x) = \begin{bmatrix} \dot{z} \\ M^{-1}(z)(-h_0(z,\dot{z}) - \partial P(z)/\partial z) \end{bmatrix} \triangleq \begin{bmatrix} \dot{z} \\ h(z,\dot{z}) \end{bmatrix}$$

$$B(x) = \begin{bmatrix} O_{2\times n_0}, & (M^{-1}(z)B_1)^T \end{bmatrix}^T$$

$h(z,\dot{z}) = -h_0(z,\dot{z}) - \partial P(z)/\partial z$

The system (2.4) together with the outputs OV_1 or OV_2 can be written as

$$\dot{x} = f(x) + B(x)u$$
$$y = Cx = [C_1 \quad O]x \tag{3.3}$$

For the choice of y according to (2.8), such that the point close to the end effector is controlled, one has

$$y = \begin{bmatrix} \rho_1 \\ \rho_e \end{bmatrix} = \begin{bmatrix} \theta_1 + \alpha_1 \frac{\delta_1(L_1,t)}{L_1} \\ \theta_1 + \frac{\theta_2}{2} + \frac{1}{2}\left(\frac{\alpha_1\delta_1(L,t)+\alpha_2\delta_2(L,t)}{L}\right) \end{bmatrix} \tag{3.4}$$

Comparing the equations (3.3) and (3.4) one obtains

$$C_1 = \begin{bmatrix} 1 & 0 & \alpha_1\frac{\phi_{11}(L_1)}{L_1}, & \cdots & \alpha_1\frac{\phi_{1n}(L_1)}{L_1} & 0 & \cdots & 0 \\ 1 & 0.5 & \alpha_1\frac{\phi_{11}(L)}{2L} & \cdots & \alpha_1\frac{\phi_{1n}(L)}{2L} & \alpha_2\frac{\phi_{21}(L)}{2L} & \cdots & \alpha_2\frac{\phi_{2n}(L)}{2L} \end{bmatrix} \tag{3.5}$$

$\triangleq$ (R, H) where R is 2×2 matrix.

Similarly, for the choice of output given by (2.9),the y matrix is

$$y = \begin{bmatrix} \rho_1 \\ \rho_2 \end{bmatrix} = \begin{bmatrix} \theta_1 + \alpha_1 \frac{\delta_1(L_1,t)}{L_1} \\ \theta_2 + \alpha_2 \frac{\delta_2(L_2,t)}{L_2} \end{bmatrix} \tag{3.6}$$

and the C_1 matrix is

$$C_1 = \begin{bmatrix} 1 & 0 & \alpha_1\frac{\phi_{11}(L_1)}{L_1} & \cdots & \alpha_1\frac{\phi_{1n}(L_1)}{L_1} & 0 & \cdots & 0 \\ 0 & 1 & 0 & \cdots & 0 & \alpha_2\frac{\phi_{21}(L_2)}{L_2} & \cdots & \alpha_2\frac{\phi_{2n}(L_2)}{L_2} \end{bmatrix} \tag{3.7}$$

$\triangleq$ (R, H) $R = I$, where R is a 2×2 identity matrix.

Here, matrices R, and H are defined in (3.5) and (3.7). We note that the matrix H is a function of α_i. The matrices R and H have different forms and depend on the choice of

output variables.

We are interested in deriving a control law such that the output $y(t)$ tracks a reference trajectory $y_r(t)$.

3.3 Variable Structure Control Law

Differentiating y and using (3.3) gives

$$\dot{y} = C_1 \dot{z}$$

$$\ddot{y} = C_1 h(z, \dot{z}) + C_1 M^{-1}(z) B_1 u \tag{3.8}$$

We shall be interested in a region of state space $\Omega \subset R^{2n_0}$ in which $B^*(z) \triangleq C_1 M^{-1}(z) B_1$ is nonsingular. Thus the tracking order of the system (3.3) is 2 and the system (3.3) and (3.8) is invertible.

Now we proceed to derive the variable structure system. The VSC law is a discontinuous function of state variables. For the design of the variable structure system (VSS), we choose a switching surface in the state space for the control function to have discontinuity, and the control law is chosen such that the trajectories of the system beginning from any initial condition are attracted towards this surface.

The switching surface is chosen of the form

$$S(\tilde{y}, \dot{\tilde{y}}) = \dot{\tilde{y}} + 2\zeta_e \omega_{ne} \tilde{y} + {\omega_{ne}}^2 w, \tag{3.9}$$

where

$\tilde{y} = (\tilde{y_1}, \dot{\tilde{y}_2})^T = (y_1 - y_{r1}, y_2 - y_{r2})^T$, $y = (y_1, y_2)^T$

y is the actual trajectory

y_r is the reference trajectory

$\tilde{y}$ is the output trajectory error

$S = (S_1, S_2)^T, \zeta_e > 0, \omega_{ne} > 0$

ζ_e is the damping coefficient

ω_{ne} is the natural frequency

The vector $w = (w_1, w_2)^T$ is the integral of the tracking error, thus

$$\dot{w} = \tilde{y}, w \in R^2 \tag{3.10}$$

In the sliding phase, once the system trajectories reach the switching surface, subsequent motion of the trajectories involves sliding of the trajectories on the surface. Therefore, in the sliding phase it can be seen that $S = 0$. Differentiating (3.9) and using (3.10), we have

$$\dot{S} = \ddot{\tilde{y}} + 2\zeta_e \omega_{ne} \dot{\tilde{y}} + {\omega_{ne}}^2 \tilde{y} = 0 \tag{3.11}$$

In sliding phase the system is asymptotically stable implying that $\tilde{y}(t) \rightarrow 0$, as $t \rightarrow \infty$, for $\zeta_e > 0, \omega_{ne} > 0$. Also, once in the sliding phase, the motion of the system trajectories is insensitive to parameter uncertainty.

Now we choose the control law such that the trajectories are attracted towards $S = 0$ when $S(\tilde{y}(0), \dot{\tilde{y}}(0)) \neq 0$. If y is the actual trajectory and y_r is the reference trajectory, then the trajectory error $\tilde{y}$ is given by $y - y_r$. Using this in equation (3.11) we obtain

$$\dot{S} = \dddot{y} - \dddot{y}_r + 2\zeta_e\omega_{ne}\ddot{\tilde{y}} + {\omega_{ne}}^2\dot{\tilde{y}} \tag{3.12}$$

Substituting for $\dddot{y}$ from (3.8) in (3.12), we have

$$\begin{aligned}\dot{S} &= C_1 h(z,\dot{z}) + B^*(z)u - \dddot{y}_r + 2\zeta_e\omega_{ne}\ddot{\tilde{y}} + {\omega_{ne}}^2\dot{\tilde{y}} \qquad (3.13)\\ &\triangleq \quad a(z,\dot{z}) + B^*(z)u\end{aligned}$$

where $a(z,\dot{z}) = C_1 h(z,\dot{z}) - \dddot{y}_r + 2\zeta_e\omega_{ne}\ddot{\tilde{y}} + {\omega_{ne}}^2\dot{\tilde{y}}$

To this end, it is assumed that

$$\begin{aligned}a(z,\dot{z}) &= a_n(z,\dot{z}) + \Delta a(z,\dot{z})\\ B^*(z) &= {B_n}^*(z) + \Delta B^*(z)\end{aligned} \tag{3.14}$$

where $a_n, {B_n}^*$ are the nominal values of a and B^* and $\Delta a, \Delta B^*$ denote uncertain portions of a and B^*, respectively.

Assumption 1: There exists functions γ_i such that

$$\begin{aligned}\|\Delta B^*(z){B_n}^{*-1}(z)\| &\leq \gamma_1(x) < \gamma_0 < 1\\ \|\Delta a(x) - \Delta B^*(z){B_n}^{*-1}(z)a_n(x)\| &\leq \gamma_2(x,t)\end{aligned} \tag{3.15}$$

We choose control law u such that $\dot{S} < 0$ if $S \neq 0$ and the trajectory reaches the surface $S = 0$ in a finite time. In view of (3.13), we select u of the form

$$u = B_n^{*-1}(z)[-a_n(x) - ksgn(S) + v] \tag{3.16}$$

where $v = (v_1, v_2)^T$ is the stabilization signal to be determined later and

$$sgn\ (S_i) = \begin{cases} 1, & S_i > 0 \\ 0, & S_i = 0 \\ -1, & S_i < 0 \end{cases}$$

Substituting (3.16) in (3.13), gives

$$\dot{S} = \Delta a(x) + \Delta B^*(z)u - ksgn(S) + v \tag{3.17}$$

where

$$sgn\ (S_i) = \begin{cases} 1, & S_i > 0 \\ 0, & S_i = 0 \\ -1, & S_i < 0 \end{cases}$$

When there is no uncertainty in the system (i.e $\Delta a = 0, \Delta B^* = 0$), (3.17) gives

$$\dot{S} = -ksgn(S) + v \tag{3.18}$$

In view of (3.18) with $v = 0$, $\dot{S} < 0$, if $S \neq 0$.

Thus when $v = 0, \dot{S} < 0$ if $S \neq 0$ and the trajectory reaches the surface $S = 0$ in finite

time. By selecting a proper value of k, one can also show using Lyapunov stability theory that the surface $S = 0$ is reached even in the presence of model uncertainty when $v = 0$. Consider a Lyapunov function

$$V(s) = |S_1| + |S_2| \tag{3.19}$$

Let us chose the gain k such that

$$k \geq (1 - \gamma_1(x))^{-1}(\delta + \gamma_2(x,t)) \tag{3.20}$$

where $\delta > 0$. Then it following Refs. 11 and 14, it can be shown that in the closed loop system with $v = 0$, one has

$$\dot{v}(t) \leq -\delta \tag{3.21}$$

for all $S \neq 0$ and $t \in [0, \infty)$. Since $v(0) > 0, S \neq 0$, it follows that indeed the trajectory reaches the surface $S = 0$ in spite of the uncertainty in the system model provided the Assumption 1 holds.

The VSC law (3.16) is a discontinuous function of x. However, discontinuity in control input causes chattering behavior, which is undesirable. It is well known that chattering can be avoided buy using a smooth approximation of the discontinuous control input. Here, for obtaining a continuous control law, we use the *sat* function instead of the *sgn* function. Thus in the control law (3.16) $sgn(S_i)$ is replaced by $sat(S_i)$ where

$$\text{sat}(S_i) = \begin{cases} 1, & S_i > \epsilon_1 \\ S_i/\epsilon_1, & |S_i| \leq \epsilon_1 \\ -1, & S_i < -\epsilon_1 \end{cases} \tag{3.22}$$

where $\epsilon_1 > 0$

Remark 1: When the system model is exactly known, in the closed-loop system including the VSC law, (3.18) holds in the reaching phase and (3.11) holds in the sliding phase. However when there is uncertainty in the system (3.11) holds after a finite time. In view of (3.11), it follows that in the closed-loop system, the responses are asymptotically linearized and the tracking error response satisfies a linear differential equation even though the system is nonlinear.

3.4 Zero Dynamics Stability and Stabilization

Using the VSC law, one can track given reference trajectories. However, this excites the elastic modes of the arm. Hence, the design of a stabilizer is necessary for the damping of the elastic oscillations and the capture of the terminal state. In the neighborhood of the terminal state, since the rigid and elastic modes result in small oscillations, the system can be well approximated by linear differential equations.

Using VSC law, the output vector can be controlled. Thus it is essential to examine the zero dynamics of the system[16-17]. The zero dynamics of the system describe the behavior

of the system when the output error vector is identically zero. In the following section only local stability will be examined.

In order to study the behavior of the internal dynamics, it will be convenient to obtain the system representation in a new state space. Further, we assume that $y_r = y_r^*, \dot{y}_r = 0, \ddot{y}_r = 0$ and that there is no uncertainty in the system. Let $x^* = (z^{*T}, 0)^T, z^* = (\theta^{*T}, q^{*T})^T$ be the equilibrium state vector. The equilibrium value of z^* is the solution of the following equation.

$$\frac{\partial P(z^*)}{\partial q} = 0$$

Let $\Delta\theta = \theta - \theta^*, \Delta q = q - q^*, \Delta y = y - y_r$. In view of (3.5) and (3.7), one has

$$\Delta y = R\Delta\theta + H\Delta q \tag{3.23}$$

We note that for the parameterization (3.7), $R = I$. Neglecting the second-order terms in $\dot{\theta}$ and $\dot{q}$, the linearized q-responses obtained from (3.1) are governed by

$$M_{21}(z^*)\Delta\ddot{\theta} + M_{22}(z^*)\Delta\ddot{q} + P_{qq}\Delta q = 0 \tag{3.24}$$

where

$$P_{qq} = \frac{\partial^2 \mathrm{P}}{\partial \mathrm{q} \partial \mathrm{q}}$$

where, the inertia matrix M is partitioned as

$$M(z) = \begin{bmatrix} M_{11}(z) & M_{12}(z) \\ M_{21}(z) & M_{22}(z) \end{bmatrix}$$

For the stability analysis, we assume that there is no uncertainty in the system. The perturbed Δy dynamics obtained from (3.9) and (3.10) are given by

$$\begin{aligned} \Delta\dot{y} &= S - 2\zeta_e\omega_{ne}\Delta y - {\omega_{ne}}^2\Delta w \\ \Delta\dot{w} &= \Delta\tilde{y} \end{aligned} \tag{3.25}$$

Using (3.25) gives

$$\Delta\ddot{y} = \dot{S} - 2\zeta_e\omega_{ne}\Delta\dot{y} - \omega_{ne}^2\Delta y \tag{3.26}$$

Using the modified continuous control law obtained from (3.16) with the *sat* function in (3.22) one has from (3.18) that

$$\dot{S} = -\frac{kS}{\epsilon_1} + v \tag{3.27}$$

when there is no uncertainty in the system.

Define the deviation in the state vector from equilibrium point ξ as

$$\xi = \begin{bmatrix} \Delta y^T & S^T & \Delta q^T & \Delta\dot{q}^T & \Delta w^T \end{bmatrix}^T \tag{3.28}$$

Then the linearized system is given by

$$\dot{\xi} = \begin{bmatrix} A_{11} & I & 0 & 0 & A_{15} \\ 0 & A_{22} & 0 & 0 & 0 \\ 0 & 0 & 0 & I & 0 \\ F_1 & F_2 & F_3 & 0 & F_4 \\ I & 0 & 0 & 0 & 0 \end{bmatrix} \xi + \begin{bmatrix} 0 \\ I \\ 0 \\ B_2 \\ 0 \end{bmatrix} v \tag{3.29}$$

$$\triangleq \tilde{A}\xi + \tilde{B}v$$

where

$\tilde{M}_{22} = (M_{22}(z^*) - M_{21}(z^*)R^{-1}H), M^*{}_{21} = M_{21}(z^*),$

$b_1 = 2\zeta_e {\omega_{ne}}^2,$

$F_1 = \tilde{M_{22}}^{-1}[{M_{21}}^* R^{-1}(-{b_1}^2 + {\omega_{ne}}^2]$

$F_2 = \tilde{M_{22}}^{-1} {M_{21}}^* R^{-1}(\frac{k}{\epsilon} + b_1)$

$F_3 = \tilde{M_{22}}^{-1}(H - P_{qq})$

$F_4 = -\tilde{M_{22}}^{-1} {M_{21}}^* R^{-1} b_1 {\omega_{ne}}^2$

$B_2 = -\tilde{M_{22}}^{-1} {M_{21}}^* R^{-1}$

$$A_{11} = \begin{bmatrix} -b_1 & 0 \\ 0 & -b_1 \end{bmatrix}$$

$$A_{15} = \begin{bmatrix} -{\omega_{ne}}^2 & 0 \\ 0 & -{\omega_{ne}}^2 \end{bmatrix}$$

$$A_{22} = \begin{bmatrix} -\frac{k}{\epsilon} & 0 \\ 0 & -\frac{k}{\epsilon} \end{bmatrix}$$

The linearized zero dynamics of the system are obtained from (3.29) when $\Delta y = 0, S =$

$0, \Delta w = 0$ and $v = 0$. Thus the zero dynamics of the system when $y = y^*_r$, are given by

$$\tilde{M}_{22}\Delta\ddot{q} + P_{qq}\Delta q = 0 \tag{3.30}$$

We note that H is a function of the parameter α_i. The stability of q-responses depends on the stability of the zero dynamics. Numerically, one can solve the characteristic equation of (3.30) which is

$$\det\left(\tilde{M}_{22}\lambda^2 + P_{qq}\right) = 0 \tag{3.31}$$

to examine the stability of the zero dynamics where *det* denotes the determinant of the matrix. It is found that for $\alpha > \alpha^*$, a critical value, the roots of (3.30) have significantly large positive real parts and q-responses diverge rapidly when $\tilde{y} = 0$

For the design of the stabilizer, α is chosen such that $\alpha \in [0, \alpha^*)$. For the final capture of the terminal state, a stabilization signal of the form

$$v = -\tilde{F}\xi \tag{3.32}$$

is chosen such that the closed-loop system matrix $\tilde{A}_c = (\tilde{A} - \tilde{B}\tilde{F})$ is Hurwitz. For the computation of $\tilde{F}$, one can use optimal control theory or pole placement technique. In this study we have chosen the design of the stabilizer using pole assignment technique. In order to obtain desirable responses, a proper selection of closed-loop poles of the matrix $\tilde{A}_c$ is essential. In view of the equations (3.25) and (3.27), the set of poles S_r associated with Δy, Δw, and S responses have negative real parts. The set of poles S_e associated with

zero dynamics (3.30) are almost on the imaginary axis for $\alpha \in [0, \alpha^*)$. A good choice of pole locations for $\tilde{A}_c$ is

$$S_{cl} = S_r \cup S_c$$

where the set S_c is given by

$$S_c = \left\{ (\nu + j\beta) : \quad \nu < 0, \quad \beta \in S_e \right\}$$

That is, in the closed-loop system, the poles associated with the zero dynamics are shifted by ν units to the left in the complex plane keeping the imaginary component unchanged.

The synthesis of the controller is as follows. First, the variable structure controller is used for large maneuvers of the arm. When the trajectory reaches the neighborhood of the terminal value, the linear stabilizer loop is closed for the capture of the terminal state and to dampen the vibrations. The stabilizer is effective if the θ and q-responses remain in a small neighborhood of the equilibrium state at the instant when the stabilizer is switched.

3.5 Digital Simulation Results

This section explores the results of the digital simulations carried out for each of two parameterizations of the end effector position. The model is highly nonlinear and includes the functions causing rigid and elastic mode interactions. The parameters assume the nominal values that are listed in the Appendix 1. The value of α is 0.4 for the both the parameterizations Also, simulation is done for $\alpha = 0.7$ for the case of parameterization denoted by OV_2. The mode shapes 'ϕ_{ij}' are selected as clamped-free modes. Assuming that the

amplitude of higher modes of the flexible links is very small when compared to the first ones, the case with $n = 2$ in the expression for elastic deflection (3.1), is illustrated.

With the choice of $n = 2$, one has the state vector x of dimension 12 where $x = (z^T, \dot{z}^T)^T$ and $z = [\theta_1, \theta_2, q_{11}, q_{12}, q_{21}, q_{22}]^T$. It can be seen that the elements of inertia matrix are functions of θ and q. Also, the following initial conditions are assumed: $y_r(0) = \dot{y_r}(0) = \ddot{y_r}(0) =$ 0 , $x(0) = 0$ and $w(0) = 0$

A command trajectory $y_r(t)$ was generated to control $y(0) = 0$ to $y_r{}^*$. It was assumed that the given tip position corresponds to $y_r^* = (90°, 120°)^T$ for the parameterization denoted by the output variable OV_1 and $y_r^* = (90°, 60°)^T$ for the parameterization denoted by the output variable OV_2.

The command trajectory was generated by a third order filter

$$\dddot{y_r} + P_2\ddot{y_r} + P_1\dot{y_r} + P_0(y_r - y^*) = 0$$

The matrices P_i of the command generator are taken as $P_i = p_i\ I_{2\times 2}$, i=0,1,2 and are selected such that the poles associated with $y_{ri}(t)$, the i^{th} component of $y_r(t)$, are at { -2, -2 $\pm$ i2 }. The parameters were selected as $k = 100$, $\zeta_e = 0.707$ $\epsilon = 0.3$ and $\omega_{ne} = 3.5$ yielding poles associated with $\tilde{y_i}$, of values -333.33, -2.47 $\pm$ i2.48 },

To examine the stability of zero dynamics the poles of (3.30) are computed for different values of α. Table 1 and Table 2 show the most significant unstable roots belonging to the

$\alpha = 0.8$	$0.000 \pm 33.68i$
$\alpha = 0.82$	$0.000 \pm 35.54i$
$\alpha = 0.84$	$0.000 \pm 37.75i$
$\alpha = 0.86$	$0.000 \pm 40.43i$
$\alpha = 0.88$	$0.000 \pm 43.77i$
$\alpha = 0.9$	$3.69 \pm 278.34i$
$\alpha = 0.92$	$88.96 \pm 278.04i$
$\alpha = 0.94$	$139.29 \pm 276.50i$
$\alpha = 0.96$	$194.91 \pm 271.69i$
$\alpha = 0.98$	$273.00 \pm 255.57i$
$\alpha = 1.$	$321.62 \pm 0.000i$

Table 3.1: Dominant Poles for parameterization OV_1

$\alpha = 0.8$	$0.000 \pm 37.83i$
$\alpha = 0.82$	$0.000 \pm 40.65i$
$\alpha = 0.84$	$0.000 \pm 44.20i$
$\alpha = 0.86$	$0.000 \pm 28.37i$
$\alpha = 0.88$	$21.68 \pm 239.02i$
$\alpha = 0.9$	$101.90 \pm 220.43i$
$\alpha = 0.92$	$164.34 \pm 181.16i$
$\alpha = 0.94$	$230.07 \pm 0.000i$
$\alpha = 0.96$	$102.91 \pm 0.000i$
$\alpha = 0.98$	$7.51 \pm 0.000i$
$\alpha = 1.$	$6.13 \pm 0.000i$

Table 3.2: Dominant Poles for parameterization OV_2

set S_e (the set of eigenvalues associated with the flexible modes), for different values of α for the parameterization OV_1 and parameterization OV_2, respectively.

It can be seen that as α increases beyond 0.86 the dynamic behavior of the zero dynamics is highly sensitive to the value of α, since the positive real part of the unstable eigenvalue rapidly increases as the value of α approaches 1. Thus a good choice of α^* is 0.86, and we must use $\alpha \in [0, \alpha^*)$ for defining the output vectors in (3.4) and (3.6). As an illustration, we have chosen $\alpha = 0.4$ for controller design.

For the chosen feedback gains, the sets S_r and S_e of poles of (3.30) for $\alpha = 0.4$ for the

choice of OV_1 are

$$S_r = [-333.33, -333.33, -2.47 \pm 2.48i, -2.47 \pm 2.48i] \tag{3.33}$$

$$S_e = [\pm 19.32i, \pm 72.85i, \pm 449.60i, \pm 460.92i]$$

and for the case denoted by OV_2 the sets S_r and S_e are

$$S_r = [-333.33, -333.33, -2.47 \pm 2.48i, -2.47 \pm 2.48i] \tag{3.34}$$

$$S_e = [\pm 19.67i, \pm 71.73i, \pm 449.73i, \pm 459.96i]$$

It can be noted that the sets of poles S_r are equal in both cases of parameterizations but the set of poles S_e is different and the poles are approximately same. The set of poles S_e is shifted by $\nu = -2.5$ in the complex plane using the stabilizer.

In the simulations that follow, y_1 and y_2 denote the chosen outputs ; $e_1 = \tilde{y}_1$ and $e_2 = \tilde{y}_2$ are the trajectory errors ; θ_1 and θ_2 are the joint angles ; u_1 and u_2 denote the control inputs ; $D_{1e} = \delta_1(L_1, t)$ the tip deflections for the two links, and $(y_{t1}, y_{t2}) = (\rho_{1t}, \rho_{et})$ for parameterization (OV_1) and $(y_{t1}, y_{t2}) = (\rho_{1t}, \rho_{2t})$ for parameterization (OV_2). Even though we denote the outputs for both parameterizations by the same notation, we note that they do not represent the same variables. It should be noted here that the outputs y_1 and y_2 are to the actual tip. The simulation results show that these outputs follow the tip positions y_{t1} and y_{t2} accurately, as the tip errors are of extremely small magnitudes, thus validating our choice. The simulation results are also shown for off

payload for both cases of parameterizations.

3.5.1 Simulation Results, Output Variable OV_1

Trajectory tracking : Control without stabilization

In this case, simulation was carried out for nominal payload and the stabilizer loop was left open with $\alpha = 0.4$ for the parameterization OV_1. The trajectory errors were found to be equal to zero and efficient tracking is evident from Fig.3. The absence of the stabilizer leads to persistent elastic mode oscillations of the tips of the two links.The θ responses depict oscillations of extremely small magnitude.

Trajectory tracking : Control with Stabilization

Nominal payload

The closed-loop system was simulated (with $\alpha = 0.4$) and the stabilizer loop is closed when the trajectory enters the neighborhood of the terminal value (3 seconds). It can be observed from Fig.4 that though the tracking error was zero prior to switching of the stabilizer, the error tends to increase after the instant of switching but dies down to zero in about 5 seconds. The stabilizer dampens out the elastic mode oscillations. The elastic deflection and the control input are found to oscillate initially. Also the θ response depicts oscillation of extremely small magnitude at the instant of switching the stabilizer. It can also be noted that the chosen output y_2 very closely follows the actual end effector position ρ_{et}.

Higher payload uncertainty

Simulations were carried for a higher payload uncertainty of 150% ($\alpha = 0.4$)(Fig.5). The

controller used here is the one that was designed with nominal parameters and the initial conditions were assumed to be zero. It can be observed that the stabilizer takes more or less the same time to dampen the oscillations as it does for the case of nominal payload. It settles down to its steady state values in about 5 seconds. It can also be noted that the control torque required in this case is larger than that required for the nominal case and so is the case with the elastic deflection. The tracking error is not zero before the stabilizer is switched on in this case, as it is in the nominal payload case. Moreover, the chosen outputs y_1 and y_2 very closely follow the actual tip positions ρ_{1t} and ρ_{et}.

Lower payload uncertainty

Simulation results for a lower payload uncertainty of 50% ($\alpha = 0.4$) are presented in this section. Selected responses are shown in the Fig.6. When compared to the higher payload uncertainty case, it can be noted that though the time taken by the system to attain steady state conditions is more or less the same, the frequency of the oscillations in the lower payload case is much higher, which is also a physical reality. Moreover, the values of the control input are lower than the higher payload case and so is the elastic deflection. Also, the chosen outputs y_1 and y_2 very closely follow ρ_{1t} and the actual end effector position ρ_{et}.

3.5.2 Simulation Results, Output Variable OV_2

Trajectory tracking : Control with Stabilization

Nominal payload

The closed-loop system defined by (3.3), (3.10), (3.16) and (3.34) was digitally simulated (with $\alpha = 0.4$) and the switching logic closes the stabilizer loop when the trajectory enters

the neighborhood of the terminal value (3 seconds). It can be observed from Fig.7 that though the tracking error was zero prior to switching of the stabilizer, the error tends to increase after the instant of switching but dies down to zero in about 5 seconds. The stabilizer dampens out the elastic mode oscillations. Also y_1 and y_2 very closely follow the actual the tip positions ρ_{1t} and ρ_{2t}.

Higher payload uncertainty

Simulations were carried for a higher payload uncertainty of 125% ($\alpha = 0.4$). The controller used here is the one that was designed with nominal parameters and the initial conditions were assumed to be zero. In comparison with the case with the parameterization OV_1 this parameterization is found to tolerate lesser uncertainty. It can be observed that the stabilizer takes more or less the same time to dampen the oscillations as it takes in case of nominal payload (Fig.8). But the trajectory error in this case is not zero before the stabilizer was switched on, as is it is in the case of nominal load. After it is switched on it dies down to zero in about 5 seconds Moreover, the chosen outputs $\rho_1 t$ and $\rho_2 t$ very closely follow the actual end effector outputs y_{t1} and y_{t2}.

Lower payload uncertainty

Simulation results for a lower payload uncertainty of 25% ($\alpha = 0.4$) are presented in this section. When compared to the case with parameterization OV_1 this parameterization is found to tolerate less lower payload uncertainty. When compared to the higher payload uncertainty case, it can be noted that though the time taken by the system to attain steady state conditions is more or less the same, the frequency of the oscillations in the lower

payload case is much higher (Fig.9), which is also a physical reality. Moreover, the values of the control input are lower than the higher payload case (Fig.8) and so is the elastic deflection and the tip deflection. Also, the chosen outputs y_1 and y_2 very closely follow the actual end effector outputs ρ_{1t} and ρ_{2t}.

3.6 Conclusions

This chapter explored the control and stabilization of the multibody system developed in the Phillips Laboratory was considered. Two Parameterizations of the controlled output variables were considered. Stability of the zero dynamics was examined. Based on the variable structure system theory control laws were derived for the control of the selected output variables. Control system includes error integral term. A smooth approximation of the discontinuous law was used for the elimination of control chattering. A linear stabilizer was designed for the final capture of the terminal state and vibration suppression. It was shown that control of a point close to the tip position gave stable zero dynamics. The complete closed-loop system was simulated on the digital computer. Extensive simulations were performed to verify the performance of the system. These results show that in the closed-loop system, for each parameterization large maneuvers of the arm and vibration suppression are accomplished by the combined action of the VSC law and the stabilizer. The controller designed using parameterization OV_1 seems to tolerate larger payload uncertainty in simulation. However, research remains to be done to find the bounds on uncertainty for stability in each case. The choice of OV_1 in design leads to a true servo system fed by neighboring end effector position error in a natural way and this is certainly important from the practical point of view.

Chapter 4

SINGULAR PERTURBATION IN CONTROL

In this chapter we introduce the singular perturbation systems and discuss its characteristic features. Furthermore, derivation of composite control law is described which combines a slow control law and a fast control law for stabilization of nonlinear systems.

4.1 Singular Perturbations

Many systems require higher-order differential equations for their realistic representation. The order of these systems is increased due to the presence of some parasitic parameters such as small time constants, masses, moments of inertia, resistances, inductances, and capacitances. These parameters are usually neglected to simplify the model. The order of the systems reduces when $\epsilon = 0$, where ϵ is the small parameter. Such a problem is called a singular perturbation problem.

The singular perturbation model of a dynamical system is a state-space model in which

the derivatives of some of the states are multiplied by a small scalar ϵ. This can be represented by

$$\dot{x} = f(x, z, \epsilon. t), x(t_0) = x^0, x \in R^n \tag{4.1}$$

$$\epsilon\dot{z} = g(x, z, \epsilon, t), z(t_0) = z^0, z \in R^m \tag{4.2}$$

where f and g are slow and fast subsystems respectively which are assumed to be continuously differentiable functions of their arguments x, z, ϵ, t. When we set $\epsilon = 0$, the dimension of the state equation reduces from $n + m$ to n because the differential equation of (4.2) degenerates into the algebraic equation

$$0 = g(x_s, z_s, 0, t) \tag{4.3}$$

where the subscript "s" is used to indicate that the variables belong to a system with $\epsilon = 0$. The model (4.1) and (4.2) is in *standard form* if equation (4.3) has $k \geq 1$ isolated real roots

$$z_s = h_i(t, x_s), i = 1, 2, \cdots, k \tag{4.4}$$

Thus, a well-defined n-dimensional reduced model will correspond to each root of (4.3). Substituting (4.4) in (4.1) the ith reduced model is obtained which is given by

$$\dot{x_s} = f(x_s, h_i(x_s, t), 0. t), x_s(t_0) = x^0 \tag{4.5}$$

The initial condition for the state variable $x_s(t)$ is the same as that for $x(t)$. The equation

(4.5) is simplified as

$$\dot{x_s} = f_s(x_s, t), x_s(t_0) = x^0 \tag{4.6}$$

The velocity of z which is $\dot{z} = g/\epsilon$ is large when ϵ is small. Therefore it rapidly converges to a root of (4.3), which is the quasi-steady-state form of (4.7). Thus, the model of (4.6) is called the *quasi-steady-state model* or *slow model.*

The interaction of slow and fast phenomena in singularly perturbed systems gives rise to two-time-scale property. For the system under consideration, the slow response is given by the reduced model (4.6) and the difference between the response of the reduced model (4.6) and that of the full model (4.1), (4.2) is the fast transient.

It can be noted that in the above equations the variable z has been eliminated from the reduced model (4.6) and is substituted by its quasi-steady-state z_s. There may be a large discrepancy between the initial value of z_s and that of z. Thus, z_s cannot be a uniform approximation of z. The best estimate is given by

$$z = z_s(t) + O(\epsilon) \tag{4.7}$$

which will hold in the interval excluding t_0, that is, for $t \in [t_1, T]$ where $t_1 > t_0$. However, the approximation of x given by x_s may be uniform and the equation

$$x = x_s(t) + O(\epsilon) \tag{4.8}$$

may hold on an interval including t_0, that is for all t in the interval $[t_0, T]$.

From the equation (4.7) it is seen that in the initial or the boundary layer interval $[t_0, t_1]$ the original variable z approaches z_s. The variable z converges to its quasi-steady-state z_s only when certain stability conditions are satisfied. These conditions are derived in the following.

Although ϵ tends to zero and $\dot{z}$ tends to infinity $\epsilon\dot{z}$ remains finite. Defining a new time variable τ as

$$\tau = \frac{t - t_0}{\epsilon}, \tau = 0 att = t_0, \tag{4.9}$$

such that

$$\begin{aligned} \epsilon\frac{dz}{dt} &= \frac{dz}{d\tau} \\ \frac{d\tau}{dt} &= \frac{1}{\epsilon} \end{aligned} \tag{4.10}$$

Using the boundary layer correction $z_f = z - z_s$ from (4.2) we obtain

$$\frac{dz_f}{d\tau} = g(x^0, z_f(\tau) + z_s(t_0), 0, t_0) \tag{4.11}$$

where x^0, t_0 are the fixed parameters and the initial condition is given by $z^0 - z_s(t_0)$. The solution of the above initial value problem is used as a boundary layer correction of (4.7) resulting in possibly uniform approximation of z as

$$z = z_s(t) + z_f(\tau) + O(\epsilon) \tag{4.12}$$

Here, $z_s(t)$ is the slow transient of z, and $z_f(\tau)$ is the fast transient of z. The equation (4.12) converges to (4.) only if the correction term $z_f(\tau)$ decays as $\tau \rightarrow \infty$ to an $O(\epsilon)$ quantity. In the slow time scale t this decay is rapid since

$$\frac{dz_f(t)}{dt} = \frac{dz_f(\tau)}{d\tau}\frac{d\tau}{dt} = \frac{1}{\epsilon}\frac{dz_f(\tau)}{d\tau} \tag{4.13}$$

The stability properties of the boundary layer system (4.11) are stated as the following assumptions:

Assumption 1

The equilibrium $z_f(\tau) = 0$ of (4.11) is asymptotically stable uniformly in x^0 and t_0, and $z^0 - z_s(t_0)$ belongs to its domain of attraction, so $z_f(\tau)$ exists for $\tau \geq 0$. Then

$$\lim_{\tau \to \infty} z_f(\tau) = 0 \tag{4.14}$$

Assumption 2

The eigenvalues of $\partial g/\partial z$, evaluated for $\epsilon = 0$ along $x_s(t), z_s(t)$, have real parts smaller than a fixed negative number, i.e.

$$Re\lambda\frac{\partial g}{\partial z} \leq -c < 0 \tag{4.15}$$

Then the following result can be stated [34].

Tikhonov's theorem:

If the Assumptions 1 and 2 are satisfied, then for all $t \in [t_0, T]$,

$$x = x_s(t) + O(\epsilon) \tag{4.16}$$

and there exists $t_1 \geq t_0$ such that all $t \in [t_1, T]$

$$z = z_s(t) + z_f(\tau) + O(\epsilon) \tag{4.17}$$

The proof of Tikhonov's theorem makes use of two-time scale asymptotic expansions of x, z having some terms defined in t-scale and others in τ-scale. For the control applications, in which Assumptions 1 and 2 are satisfied, this approach is applicable.

4.2 Composite Control Law

For the control of the elastic spacecraft considered in this thesis, composite control method is used. In this method the original singularly perturbed system is decomposed into two subsystems in separate time scales: the low-order slow subsystem and a boundary layer fast subsystem. Thus, it takes advantage of the singularly perturbed nature of the original problem. Controllers are designed for each lower-order subsystem and a composite state feedback control is obtained by combining the slow and fast control laws. In this section the derivation of the Composite Control law is described.

Consider a standard singularly perturbed systm given by

$$\dot{x} = f(x, z, v), x \in R^n \tag{4.18}$$

$$\epsilon \dot{z} = g(x, z, v), z \in R^m \tag{4.19}$$

where $v \in R^r$ is a control input. Although one can consider g as a nonlinear function in z and v, it will be seen later that for the spacecraft model considered in this thesis g is a linear function in z and v. Hence one has

$$g(x,z,v) = a_2(x) + A_2(x)z + B_2(x)v \tag{4.20}$$

Since the system is assumed to be a standard singularly perturbed system for every $v \in B_v \subset R^r$, one has

$$0 = a_2(x_s) + A_2(x_s)z_s + B_2(x_s)v_s \tag{4.21}$$

where the subscript "s" indicates that the variables belong to a system with $\epsilon = 0$. This equation has a unique root z_s in $B_x \times B_z \times B_v$ if $A_2(x)$ is nonsingular.

The composite control v is given by the sum of slow control (v_s) and the fast control (v_f).

$$v = v_s + v_f \tag{4.22}$$

4.2.1 Slow problem

For the slow subproblem, the fast transient is neglected. From (4.21), since A_2^{-1} is assumed to exist, one has

$$z_s(x_s) = -A_2^{-1}(x)(a_2(x_s) + B_2(x_s)v_s) \triangleq h(x_s, v_s) \tag{4.23}$$

Substituting (4.24) in (4.19), one obtains the reduced order slow subsystem

$$\dot{x}_s = f(x_s, h(x_s, v_s), v_s) \triangleq f_s(x_s, v_s) \tag{4.24}$$

For the stabilization of the system (4.25), one derives a control law of the form

$$v_s = \Gamma_s(x_s) \tag{4.25}$$

We note that the slow control law is only a function of slow variable x_s.

The slow control v_s is designed for the slow subsystem (4.25) such that $x_s = 0$ is its asymptotically stable equilibrium.

4.2.2 Fast subproblem

Differentiating the boundary layer correction equation (4.11) and multiplying it by ϵ one has

$$\epsilon z_f' = \epsilon \dot{z} - \epsilon z_s' \tag{4.26}$$

and substituting equation (4.21) for $\epsilon \dot{z}$ and using (4.23) and (4.11) in (4.27) we obtain

$$\epsilon z_f' = a_2(x) + A_2(x)z + B_2(x)v - \epsilon z_s' \tag{4.27}$$

Since x is the slow variable, substituting x_s for x in (4.28), one has

$$\epsilon z_f' = a_2(x_s) + A_2(x_s)[z_f + z_s] + B_2(x_s)(v_s + v_f) - \epsilon z_s' \tag{4.28}$$

Neglecting the $\epsilon z_s'$ terms for small ϵ and using the equation (4.24) in (4.28) we obtain the fast subproblem as

$$\epsilon z_f' = A_2(x_s)z_f + B_2(x_s)v_f \tag{4.29}$$

Noting that, $\epsilon \dot{z_f} = dz_f/d\tau$, one has

$$\frac{dz_f}{d\tau} = A_2(x_s)z_f + B_2(x_s)v_f \tag{4.30}$$

For the stabilization of the system (4.30) one derives the control law of the form

$$v_f = \Gamma_f(x_s, z_f) \tag{4.31}$$

The fast control law is designed such that

1. $\Gamma_f(x_s, h(x_s, \Gamma_s(x_s))) = 0$
2. $z = h(x_s, \Gamma_s(x_s))$ is an asymptotically stable equilibrium of the closed loop boundary layer system of (4.30).

Using optimal control theory a linear feedback control law for stabilizing the system (4.29) can be derived. The performance index for minimization is chosen as

$$J_f = \int_0^\infty (z_f' Q(x_s) z_f + v_f' R v_f) dt \tag{4.32}$$

To find the optimal solution to the fast subproblem the following controllability assumption is made

Assumption 3

For every fixed $x \in D$, a neighborhood of $x = 0$

$$rank[B_2, A_2B_2, \cdots, A_2^{m-1}B_2] = m \tag{4.33}$$

For each $x \in D$, the optimal control law is given by

$$\Gamma_f(z_f, x_s) = -R^{-1}(x_s)B_2'(x_s)P_f(x_s)z_f \tag{4.34}$$

where P_f is the positive definite solution of the Riccati equation

$$0 = P_f A_2 + A_2' P_f - K_f B_2 R^{-1} B_2' P_f + Q \tag{4.35}$$

Since the control (4.36) stabilizes the fast subsystem one has

$$\epsilon \dot{z_f} = (A_2 - B_2 R^{-1} B_2' P_f) z_f \triangleq \bar{A}_2(x_s) z_f \tag{4.36}$$

and $Re\gamma[\bar{A}_2(x_s)] < 0$ for every $x_s \in D$.

The composite control law is obtained by substituting (4.36) in (4.33) as

$$v(x_s, z) = \Gamma_s(x_s) - R^{-1} B_2' P_f z_f \tag{4.37}$$

Since $z_f = z - z_s$ one has

$$v(x_s, z) = \Gamma_s(x_s) - R^{-1} B_2' P_f (z - z_s) \tag{4.38}$$

In order to synthesize the controller using the actual state variable, one substitutes x for x_s in (4.39) to obtain (4.40).

$$v(x, z) = \Gamma_s(x_s) - R^{-1} B_2' P_f (z + A_2^{-1}(x)(a_2(x) + B_2(x)\Gamma_s(x)) \tag{4.39}$$

It can be proved that if Assumption 3 is satisfied then there exists ϵ^* such that for every $\epsilon \in (0, \epsilon^*]$, the composite control v defined in (4.40) stabilizes the full system (4.19), (4.20)

in a sphere centered at $x = 0, z = 0$ [33].

The next chapter describes the application of singular perturbation control derived in this chapter to the attitude control of spacecraft.

Chapter 5

CONTROL OF ELASTIC SPACECRAFT BY NONLINEAR INVERSION AND SINGULAR PERTURBATION

5.1 Introduction

In this chapter, we consider rotational maneuver and stabilization of an elastic spacecraft(orbiter-beam-tip body configuration) shown in Fig.2.

The chosen output vector consists of the pitch angle, and the first two dominant elastic modes of the beam. Based on nonlinear inversion an inverse control law is derived to decouple the output from the remaining fast elastic dynamics. Decoupling of output responses results in a standard singular perturbation model of the spacecraft. Using singular

perturbation theory, the spacecraft dynamics are decomposed into a low-order slow subsystem, and a boundary layer fast subsystem. The decoupled attitude angle and the dominant elastic modes are the components of the slow state vector and the remaining elastic modes are included in the fast state vector. Based on singular perturbation theory, controllers are designed for each lower-order subsystem. The slow controller is designed based on the slow subsystem, and the fast controller is derived using the boundary layer model which describes the deviation of the fast elastic modes from their quasi-steady-state values. Then a composite state feedback control is obtained by combining the slow and the fast control laws.

In this study it is assumed that all the state variables are available for feedback. In the practical situation one can design a state estimator for constructing the unmeasurable state variables using the signals from the sensors such as accelerometers, and strain gauges, etc.

In the following sections the attitude control of the elastic spacecraft is described in detail.

5.2 Problem Formulation

The mathematical model of the elastic spacecraft has been presented in Chapter 2. The equations of motion are given by equation (2.12) as

$$\begin{pmatrix} D_{11} & D_{12} \\ D_{12}^T & D_{22} \end{pmatrix} \begin{bmatrix} \ddot{\theta} \\ \ddot{p} \end{bmatrix} = \begin{bmatrix} 0 \\ g \end{bmatrix} \dot{\theta}^2 - \begin{bmatrix} 0 \\ K \end{bmatrix} p + B_0 u \tag{5.1}$$

where, $p = (p_1, \cdots, p_m) \in R^m$ and the positive definite symmetric inertia matrix is $D \triangleq (D_{ij}), i, j = 1, 2$. Here the matrix B_0 can be obtained by equating similar terms in (2.10)

and (2.12), and

$$\mathrm{K}=\mathrm{diag}(\ \Omega_i{}^2), i = 1, \cdots, m$$

$$\mathrm{g}=(\mu_0 a_2/L)(u_{31}, \cdots, u_{3m})^T$$

Define $H \triangleq D^{-1}$, and $z = (\theta, p^T)^T \in R^{(m+1)}$. Then solving (2.12), gives

$$\ddot{z} = H_2 g\dot{\theta}^2 - H_2 K p + H B_0 u \tag{5.2}$$

where $H = [H_1, H_2]$, and H_1 denotes the first column of H.

Suppose that a third order reference model

$$\dddot{\theta}_r + 3\lambda_c\ddot{\theta}_r + 3\lambda_c{}^2\dot{\theta}_r + \lambda_c{}^3\theta_r^* = 0 \tag{5.3}$$

is given where $\lambda_c > 0$ and θ^* is the determined value of the pitch angle. The characteristic polynomial of (2.14) is

$$(\lambda + \lambda_c)^3 = 0 \tag{5.4}$$

Since $\lambda_c > 0$, the system (2.14) is asymptotically stable.

We are interested in deriving a control system such that in the closed-loop system, the attitude angle $\theta(t)$ tracks the reference trajectory $\theta_r(t)$, and the elastic oscillations are damped out.

5.3 Inversion and Singular Perturbation

In this section, nonlinear inversion of a selected input-output map will be considered, and, for the control system design, a singular perturbation model of the spacecraft will be obtained. To this end, a judicious choice of output vector consisting of θ, and first two elastic modes (p_1, p_2) is made. This choice of output variables is motivated by the fact that our objective is to control the attitude angle θ, and p_1, p_2 are the dominant modes contributing to elastic deformation of the beam. Define the output vector $y \in R^3$, by

$$\begin{aligned} y &= (\theta, p_1, p_2)^T \\ &= Cz \end{aligned} \tag{5.5}$$

where C = [I, 0]. Here I and 0 denote identity and null matrices of appropriate dimensions.

Now we consider the inversion of the input(u)-output(y) map. Following the algorithm of inversion[16], we differentiate the output y until the control input appears in its derivative first time. Differentiating $y(t)$ twice along the solution of (5.2), gives

$$\ddot{y} = CH_2 g\dot{\theta}^2 - CH_2 K p + CHB_0 u \tag{5.6}$$

For the spacecraft model, the 3×3 matrix CHB_0 is nonsingular; and thus the relative degree of the output y is 2[16]. For decoupling the dynamics of y, in view of (5.6), we choose an inverse control law of the form

$$u = (CHB_0)^{-1}[-CH_2 g\dot{\theta}^2 + CH_2 K p + v] \tag{5.7}$$

where $v \in R^3$ is a new control input. The control input v will be determined later. Substi-

tuting the control law (5.7) in (5.6), gives the integrator decoupled subsystem

$$\ddot{y} = v \tag{5.8}$$

The closed-loop system (5.2) and (5.8) has a representation of the form

$$\begin{aligned} \ddot{y} &= v \\ \ddot{p_f} &= H_{1b} g \dot{\theta}^2 - H_{1b} K p + H_b B_0 u \end{aligned} \tag{5.9}$$

where $p_f = (p_3, \cdots, p_m)^T \in R^{(m-2)}$; and H_{1b} and H_b are the submatrices obtained by deleting the first 3 rows of H_2, and H, respectively. Substituting (5.7) in (5.9), gives

$$\ddot{y} = v \tag{5.10}$$

$$\ddot{p_f} = [H_{1b} - B_1] g \dot{\theta}^2 - K_f p_f - K_{of} \bar{p} + H_b B_0 (C H B_0)^{-1} v \tag{5.11}$$

where $\bar{p} = [p_1, p_2]^T$, $B_1 \triangleq H_b B_0 (C H B_0)^{-1} C H_2$, and $[K_{of}, K_f] = [H_{1b} - B_1] K$ where K_{of} has first 3 columns of $(H_{1b} - B_1) K$.

The characteristic polynomials, associated with (5.10) and the linearized system obtained from (5.11), are given by

$$det(I\lambda^2) = \lambda^6 = 0 \tag{5.12}$$

$$det(\lambda^2 I + K_f) = 0 \tag{5.13}$$

where det(.) denotes the determinant of the matrix (.). For the spacecraft model K_f is large since K is large.

In view of (5.12) and (5.13), the poles of the system (5.10) are at the origin and the

poles of the system (5.11) are far away from the origin in the complex plane. Such a wide separation of poles of the system (5.10) and (5.11) indicates that $(y, \dot{y})$ are the slow variables and $(p_f, \dot{p_f})$ are the fast variables, and a singular perturbation model of the system (5.10) and (5.11) can be naturally obtained.

As it will be seen later that for the spacecraft model, the matrix K_f has extremely large diagonal elements compared to its off-diagonal elements. We choose the singular perturbation parameter $\epsilon > 0$ such that ϵ^2 is close to the reciprocal of the smallest diagonal element of the matrix K_f. Such a choice has also been made in [39] related to robotic arm control problem.

Define

$$K_d = \epsilon^2 K_f \tag{5.14}$$

We also introduce a new variable defined as $z_f = p_f/\epsilon^2$. Then the system (5.10) and (5.11) can be written as

$$\begin{aligned} \ddot{y} &= v \\ \epsilon^2 \dot{z_f} &= N\dot{\theta}^2 - K_d z_f - K_{of}\bar{p} + B_2 v \end{aligned} \tag{5.15}$$

where $N = (H_{1b} - B_1)g$, and $B_2 = H_b B_0 (CHB_0)^{-1}$, and $K_d = \epsilon^2 K_f$. Defining $x = (y^T, \dot{y}^T)^T \in R^6$, $\xi = ({\xi_1}^T, {\xi_2}^T)^T = (z_f^T, \epsilon \dot{z_f}^T)^T \in R^{(2m-4)}$, a state variable representation of (5.15) is given by

$$\begin{aligned} \dot{x} &= (\dot{y}^T, v^T)^T \\ \epsilon\dot{\xi} &= f(\dot{\theta}, y) + A\xi + Bv \end{aligned} \tag{5.16}$$

where $f = [0, N^T]^T \dot{\theta}^2 - [0, K_f^T]^T \bar{p}$, and

$$A = \begin{bmatrix} 0 & I \\ -K_d & 0 \end{bmatrix},$$

$$B = \begin{bmatrix} 0 \\ B_2 \end{bmatrix}.$$

The system (5.16) represents the singular perturbation model of the spacecraft. In this system, x, and ξ are the slow and the fast variables, respectively. Now the system (5.16) will be used for the derivation of the composite control law.

5.4 Composite Control Law

In this section a composite control law v will be derived based on the theory presented in Chapter 4, for rotational maneuver and vibration suppression of the elastic spacecraft.

Let the composite control law be given by

$$v = v_s + v_f \tag{5.17}$$

where v_s and v_f are the slow and the fast components of v, respectively.

5.4.1 Slow Control Law

Since $x = (y^T, \dot{y}^T)^T$, the slow system obtained from (5.16) is given by

$$\ddot{y}_s = v_s \tag{5.18}$$

where $y_s = (\theta_s, p_{1s}, p_{2s})^T$. Here subscript 's' indicates that these variables are the slow

components of the respective variables.

For the linear system (5.18), one can easily choose a control law of the form

$$v_s = \begin{pmatrix} \ddot{\theta}_r \\ 0 \\ 0 \end{pmatrix} - 2\zeta\omega_n \begin{pmatrix} \dot{\theta}_s - \dot{\theta}_r \\ \dot{p}_{1s} \\ \dot{p}_{2s} \end{pmatrix} - {\omega_n}^2 \begin{pmatrix} \theta_s - \theta_r \\ p_{1s} \\ p_{2s} \end{pmatrix} \tag{5.19}$$

for the rotational maneuver and the stabilization of the dominant modes p_1 and p_2. Substituting (5.19) in (5.18), gives the linear tracking error dynamics of the form

$$\ddot{\tilde{y}}_s + 2\zeta\omega_n\dot{\tilde{y}}_s + {\omega^2}_n\tilde{y}_s = 0 \tag{5.20}$$

where $\tilde{y}_s = y_s - y_r$, and the reference trajectory is $y_r = (\theta_r, 0, 0)^T$. With the choice of $\zeta > 0, \omega_n > 0$, the equilibrium point $(\tilde{y}_s = 0, \dot{\tilde{y}}_s = 0)$ of (5.20) is exponentially stable and $y_s(t) \rightarrow y_r(t)$ as $t \rightarrow \infty$. Note that this choice of y_r results in the convergence of (p_{1s}, p_{2s}) to $(0,0)$, as $t \rightarrow \infty$. Now, we consider the derivation of the fast control law for the control of p_f following the singular perturbation theory.

5.4.2 Fast Control Law

The quasi-steady-state $\xi_s = ({\xi_{1s}}^T, {\xi_{2s}}^T)^T$ of the fast variable ξ is obtained by setting $\epsilon = 0$ in (5.16). With $\epsilon = 0$, (5.16) becomes

$$f_s + A\xi_s + Bv_s = 0 \tag{5.21}$$

where $f_s = ({\dot{\theta}_s}^2, y_s)$

From (5.21), it follows that

$$\begin{aligned} \xi_{2s} &= 0 \\ N\dot{\theta}_s - K_d z_{fs} - K_{of}\bar{p}_s + B_2 v_s &= 0 \end{aligned} \tag{5.22}$$

Solving (5.22), gives the quasi-steady-state of ξ which is

$$\begin{aligned} \xi_{2s} &= 0 \\ \xi_{1s} = z_{fs} &= {K_d}^{-1}(N\dot{\theta}_s^2 - K_{of}\bar{p}_s + B_2 v_s) \end{aligned} \tag{5.23}$$

Thus $\xi_s = ({\xi_{1s}}^T, {\xi_{2s}}^T)^T = ({z_{fs}}^T, 0)^T$.

The deviation of the fast variable from its quasi-steady-state is given by

$$\tilde{\xi} = \begin{bmatrix} \xi_1 - \xi_{1s} \\ \xi_2 - \xi_{2s} \end{bmatrix} = \begin{bmatrix} \xi_1 - {K_d}^{-1}(N\dot{\theta}_s^2 - K_{of}\bar{p}_s + B_2 v_s) \\ \xi_2 \end{bmatrix} \tag{5.24}$$

Differentiating $\tilde{\xi}$ in (5.24) and setting the term $\epsilon\dot{\xi}_s$ associated with the derivative of slow variable to zero, gives

$$\begin{aligned} \epsilon\dot{\tilde{\xi}} &= \epsilon\dot{\xi} \\ &= f(\dot{\theta}, y) + A(\tilde{\xi} + \xi_s) + B(v_s + v_f) \end{aligned} \tag{5.25}$$

Since $\dot{\theta}$ and y are components of the slow variable x, setting $\dot{\theta} = \theta_s$ and $y = y_s$ using (5.21) in (5.25), gives

$$\epsilon\dot{\tilde{\xi}} = A\tilde{\xi} + Bv_f \tag{5.26}$$

Letting $\tau = t/\epsilon$, (5.26) gives

$$\frac{d\tilde{\xi}}{d\tau} = A\tilde{\xi} + Bv_f \tag{5.27}$$

The boundary layer model (5.27) represents the fast dynamics of the spacecraft. We are interested in deriving a fast control v_f such that the equilibrium point $\tilde{\xi} = 0$ of the system (5.27) is exponentially stable. For the spacecraft model, the system (5.27) is controllable and one can derive a linear feedback control law using linear optimal control theory for the regulation of $\tilde{\xi}(t)$ to the origin. The performance index for minimization is chosen as

$$J = \int_0^\infty (\tilde{\xi}^T Q \tilde{\xi} + \tilde{v_f}^T R \tilde{v_f}) dt \tag{5.28}$$

where Q and R are symmetric positive definite matrices. Then the optimal control law is obtained as [41]

$$\begin{aligned} F &= -R^{-1} B^T P \\ v_f &= F\tilde{\xi} = F_1(\xi_1 - \xi_{1s}) + F_2 \xi_2 \end{aligned} \tag{5.29}$$

where the feedback matrix $F = (F_1, F_2)$, and the positive definite symmetric matrix P is the unique solution of the Riccati equation

$$A^T P + PA - PBR^{-1} B^T P + Q = 0 \tag{5.30}$$

Now the composite control law (5.17) for the rotational maneuver and vibration suppression is obtained by combining the slow and the fast controllers.

For obtaining the realizable composite control, one needs to express v_s and v_f as func-

tions of actual state variables. Substituting $(y, \dot{y})$ for $(y_s, \dot{y}_s)$ in (5.19) and (5.29), gives

$$\begin{aligned} v_s &= \ddot{y}_r - 2\zeta\omega_n\dot{\tilde{y}} - {\omega_n}^2\tilde{y} \\ v_f &= F\tilde{\xi} = F_1[\xi_1 - K_d^{-1}(f(\dot{\theta}, y) + B_2 v_s)] + F_2\xi_2 \end{aligned} \tag{5.31}$$

where $\tilde{y} = (y - y_r), \dot{\tilde{y}} = (\dot{y} - \dot{y}_r)$. Then the composite control $v = v_s + v_f$ is given by

$$v = (I - F_1 K_d^{-1} B_2)(\ddot{y}_r - 2\zeta\omega_n\dot{\tilde{y}} - {\omega_n}^2\tilde{y}) + F_1(\xi_1 - K_d^{-1} f(\dot{\theta}, y)) + F_2\xi_2 \tag{5.32}$$

For obtaining the complete control u, one substitutes (5.32) for v in the inverse control law (5.7).

Based on a result of [34], one can show that the complete closed-loop system (5.1), (5.7) and (5.32) is exponentially stable for $\epsilon \in [0, \epsilon^*]$, where $\epsilon^* > 0$ is sufficiently small. The results presented in the next section indeed confirm that the closed-loop system is exponentially stable and in the closed-loop system, rotational maneuver and vibration suppression are accomplished. Furthermore, in the closed-loop system, Tikhonov's theorem guarantees that for the initial conditions of the system in the neighborhood of the slow manifold given by (5.23), the state vector of the full system can be approximated by

$$\begin{aligned} (y(t), \dot{y}(t)) &= (y_s(t) + O(\epsilon), \dot{y}_s(t) + O(\epsilon)) \\ \xi(t) &= \xi_s(t) + \tilde{\xi}(t/\epsilon) + O(\epsilon) \end{aligned}$$

where $\tilde{\xi}_s(\tau)$ is the solution of the boundary layer model (5.27).

5.5 Simulation Results

In this section, numerical results for the closed-loop system are presented. For obtaining numerical results, five significant modes are retained in the model (2.10), thus we have $m = 5$. The parameters of the spacecraft are given in the appendix. The output vector chosen is $y = (\theta, p_1, p_2)^T$. Using these parameters, the matrix associated with the fast variable $p_f = (p_3, p_4, p_5)^T$ in the closed-loop system (5.11) including the inverse controller (5.7) is computed to yield

$$K_f = \begin{bmatrix} -123.43 & -0.7055 & -1.7521 \\ 0.1284 & -527.99 & 1.0121 \\ -0.1544 & -0.4897 & -1695.52 \end{bmatrix}$$

As predicted, the matrix K_f has diagonal elements of extremely large magnitude compared to its off-diagonal elements. Let $\epsilon_1 = (123.43)^{-1/2}$ which is the reciprocal of the square root of the absolute value of the smallest diagonal element of K_f. Then we choose $\epsilon = 0.1 \approx \epsilon_1$ for the purpose of controller design.

The parameters of the slow controller are chosen as $\zeta = 0.7$, $\omega_n = 1.5$. With these values, the eigen values of the subsystem (5.20) are (-1.05 $\pm$1.07i). For the stabilization of the fast system using optimal control theory, the matrices Q and R are chosen as

$$Q = \text{diag}\begin{bmatrix} 1.0 & 1.0 & 1.0 & 0.85 & 0.85 & 0.85 \end{bmatrix}$$

$$R = \text{diag}\begin{bmatrix} 400.0 & 100.0 & 10.0 \end{bmatrix}$$

The feedback matrix F in (5.29) is

$$F = \begin{bmatrix} 0.0 & 0.0027 & -0.0049 & -0.0\,061 & 0.0049 & -0.0057 \\ 0.0003 & 0.0032 & -0.0071 & 0.0075 & 0.0083 & -0.0088 \\ -0.0034 & 0.1871 & -0.3144 & -0.4050 & 0.3098 & -0.2872 \end{bmatrix}$$

and the poles of the closed-loop fast boundary layer system (5.26) and (5.29) are obtained by computing the eigen values of $[(A+BF)/\epsilon]$ which are -2.638 $\pm$11.107i, -1.707 $\pm$ 22.927i, and -1.177 $\pm$ 41.161i. These values of the feedback parameters were selected after several trials by observing the simulated responses.

The initial conditions chosen are such that $(\theta(0), p_i(0)) = 0, (\dot{\theta}(0), \dot{p}_i(0)) = 0, \theta_r(0) = \dot{\theta}_r(0) = \ddot{\theta}_r(0) = 0$, $(i = 1, \cdots, 5)$. The chosen terminal value of θ is $\theta^\star = 100^0$ and $y_r = (\theta_r, 0, 0)^T$. The command trajectories for $p_1(t)$, and $p_2(t)$ are identically zero. Command trajectories are generated by (5.3) by choosing $\lambda_c = 1.0$. In the figures, ω denotes $\dot{\theta}$, $u_e = \delta_e(L,t)$ is the transverse deflection of the end point of the beam, and the pitch angle tracking error is $e = \theta - \theta_r$.

5.5.1 Rotational Maneuver : Fast Control Loop Open

The closed-loop system (2.10), (5.7) and (5.32) was simulated with $F = 0$. Thus the fast control loop was not closed, i.e., we have set $v_f = 0$. The poles of the open loop boundary layer system (5.27) (i.e. the eigen values of A/ϵ) are $\pm$11.110i, $\pm$ 22.978i, and $\pm$41.177i. Since the poles of (5.27) are imaginary, oscillatory responses for p_f were obtained. However, we observed smooth attitude control and the first two elastic mode responses remained identically zero. Fig.10 shows the θ and u_e responses.

5.5.2 Rotational Maneuver and Vibration Damping

The fast control loop was closed and the complete closed-loop system (2.10), (5.7), and (5.32) was simulated. The feedback parameters and initial conditions of case 5.1 were retained. Selected responses are shown in Fig.11. Smooth control of attitude was accomplished and the elastic modes converged to zero. The θ-response time of the order of 8 seconds was obtained. Maximum magnitude of end point deflection was 1.2m.

5.5.3 Rotational Maneuver and Vibration Damping with Initial Rate

To examine the effect of nonzero initial angular velocity of the spacecraft, simulation was done assuming that $\dot{\theta}(0) = \omega(0) = -5^0/s$. The remaining parameters of case 5.2 were retained. Selected responses are shown in Fig.12. We observe that in spite of the initial angular velocity, pitch angle was controlled to the desired value and elastic oscillation was suppressed. Since the spacecraft has negative initial angular velocity, larger control magnitude is required as expected.

Simulation was also done with $\dot{\theta}(0) = \omega(0) = 5^0/s$. Smooth responses were obtained. However, in this case maximum magnitude of the control input was found to be (3.25E6 Nm, 8000 Nm, 14900 N). Smaller control magnitude is required, since spacecraft has positive initial angular velocity. The results are shown in Fig.13.

5.5.4 Rotational Maneuver and Vibration Damping : Slower Command

In order to reduce the control magnitude, a slower command trajectory was generated using $\lambda_c = 0.7$ instead of $\lambda_c = 1.0$ of case 5.2. The remaining parameters of case 5.2 were retained and all the initial conditions were assumed to be zero as in case 5.2. Selected responses

are shown in Fig.14. We observe smooth control of attitude angle and stabilization of elastic modes. The response time of the order 10 second was obtained which is larger than that obtained in case 5.2. However, smaller control magnitudes were required as predicted. Moreover maximum end deflection of only 0.6m was observed.

5.6 Conclusions

In this chapter, based on nonlinear inversion and singular perturbation theory, a control system design approach for large angle rotational maneuvers of elastic spacecraft was presented. An inverse control law was derived to decompose the spacecraft dynamics into a slow subsystem and a fast subsystem. Based on these two decomposed lower order models, slow and fast controllers were designed. Slow controller was designed to track any given reference trajectory of the pitch angle and to regulate the two dominant elastic modes. Fast controller was designed to regulate the remaining elastic modes to their quasi-steady state. A composite controller was formed by combining the slow and fast controllers. In the closed-loop system composite control law accomplished smooth large angle rotational maneuvers and vibration suppression.

Chapter 6

CONCLUSIONS

This thesis deals with the question of control of two elastic dynamical systems. For the first system (the elastic multibody system developed in Phillips Laboratory, Edwards Air Force Base, CA) a Variable structure controller was designed for the control of the desired output. For the design of attitude control system for the second system (flexible spacecraft), a control law based on nonlinear inversion and for the control of the pitch angle. Simulation results show that the designed control system accomplishes the trajectory tracking and vibration suppression in both cases.

The Variable Structure controller designed for the multibody system is robust and precise trajectory tracking and vibration suppression are accomplished in spite of the payload uncertainty. The controller is found to tolerate a higher payload uncertainty of 150% and lower payload uncertainty of 50% for the parameterization OV_1 and a higher payload uncertainty of 125% and lower payload uncertainty of 25% for the parameterization OV_2. The Variable Structure law is discontinuous and causes the excitation of elastic modes of the links. The stabilizer design in this case is complicated.

Singular perturbation is a new technique in control systems design. It modifies the original ill-conditioned problem to a well-conditioned one by decomposing it into slow subproblem and a fast subproblem, thus simplifying the design. We have not considered the payload uncertainty in this case.

The approach developed in this thesis for the control of the single-axis maneuver of flexible spacecraft can be extended to three-axis rotational maneuver. The study related to the robustness of the controller for the attitude control of the spacecraft needs to be done. Also the questions related to spillover, state estimation, sensor and actuator dynamics and sensor noise are quite important. This is left as a future work.

APPENDIX 1 PARAMETER VALUES FOR TWO LINK ELASTIC ARM

Listed below are the parameter values for the two-link elastic robotic arm for which the digital simulations were carried out :

Mass of each Link	=	.58 kg
Stiffness of each link	=	466.9 Nm^2
Length of each link	=	1.0 m
Joint mass at Joint 2	=	.0012 kg
Nominal payload	=	.325 kg
Inertia of payload	=	5.241 kgm^2
Inertia of mass at Joint 1	=	0.00217 kgm^2
Inertia of mass at Joint 2	=	0.01934 kgm^2

APPENDIX 2 PARAMETER VALUES FOR ELASTIC SPACECRAFT

Following are the parameters of the elastic spacecraft:

System Parameters

m_0, m_t = (98739.5, 875.32) - Spacecraft, tip body mass(kg)

I_0, I_t = (9769869.5, 1400.512) - Spacecraft and tip body moment of inertia about their mass centers perpendicular to plane of motion (kg - m^2)

$a = (a_1, a_2)$=(2, 0.1) - Vector from spacecraft mass center to beam attachment point (m)

d = 2 - Distance of tip body mass center from the attachment point of tip body with beam (m)

ρ = 21.883 - mass per unit length of beam (kg/m)

EI = 353520 - Bending rigidity ($N - m^2$)

$m_1 = \rho L + m_t, m = m_0 + m_1, \mu_0 = m_0/m, \mu_1 = m_1/m$

$b_1 = \{(\rho L^2/2) + m_t(L + d)\}/m_1$, L = 20.0m

$a_{00} = \frac{I_0+J_0}{\rho L^3} + (m/\rho L)\mu_0\mu_1\left(\frac{a_1^2}{L^2} + \frac{a_2^2}{L^2} + \frac{2a_1b_1}{L^2}\right) - \frac{m}{\rho L^3}\mu_1^2 b_1^2$

$a_{1k} = \frac{\mu_0 a_1 u_{3k}}{L} + u_{4k} - \frac{\mu_1 b_1 u_{3k}}{L} (k = 1, 2, \cdots)$

b_{01}= $1/(\rho L^3)$

$b_{03} = \left(\mu_0\frac{a_1}{L} + 1 + \frac{d}{L} - \mu_1\frac{b_1}{L}\right)/\rho L^2$

$b_{i2} = u_{1i}/\rho L^3, b_{i3} = \{u_{2i}/\rho L^3\} - \{u_{3i}/mL\}$

Modal Parameters

$(u_{11}, \cdots, u_{15})$=(0.9087, −4.835, 6.0703, −4.966, 3.5599)

$(u_{21}, \cdots, u_{25})$=(0.676, −0.1266, −0.0027, 0.0552, −0.0608)

$(u_{31}, \cdots, u_{35})$=(1.5691, 0.5224, 0.298, 0.2204, 0.1707)

$(u_{41}, \cdots, u_{45})$=(1.654, 0.14854, 0.05058, 0.02590, 0.015)

Frequencies

$(\Omega_1, \cdots, \Omega_5)$=(0.323, 3.805, 11.10, 22.987, 41.162)

Elastic deflection

$$u_e = \sum_{j=1}^{5} (Lu_{2k} - du_{1k}) p_k(t)$$

List Of Figures

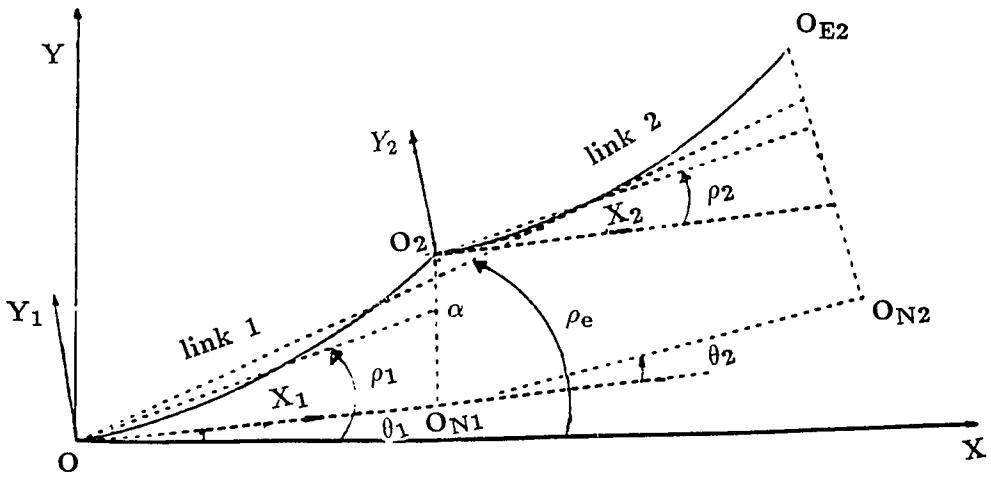

Fig.1 Model of the Robotic arm

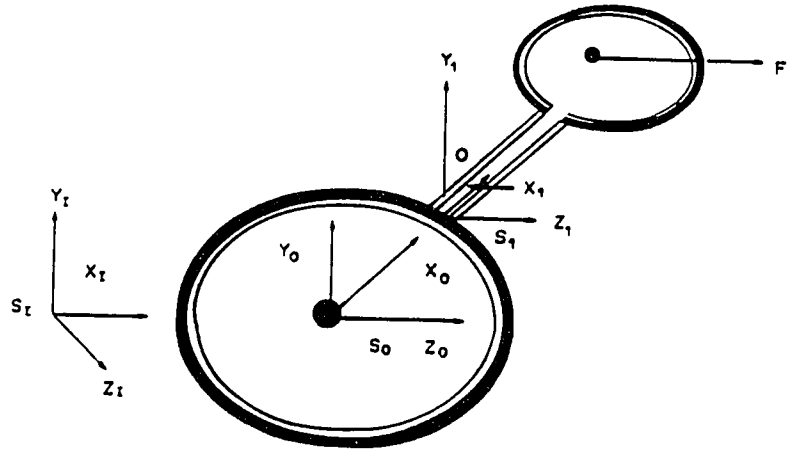

Fig.2 Model of the Elastic Spacecraft

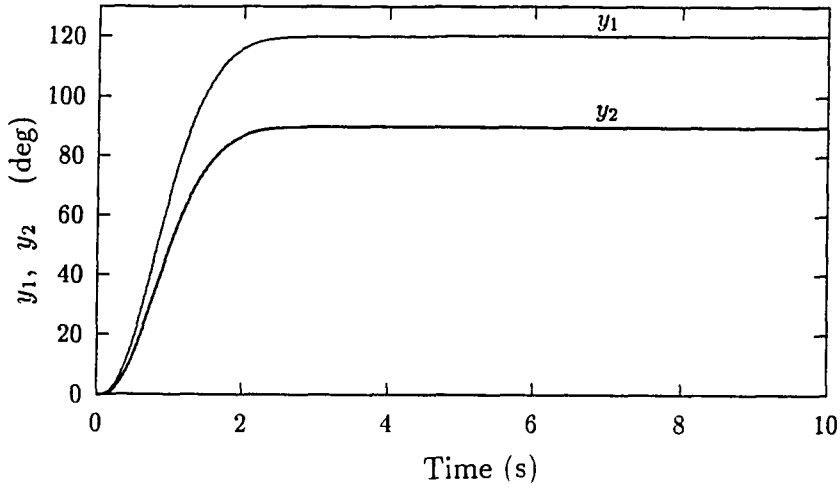
y_1
y_2
120
100
80
60
40
20
0
y_1, y_2 (deg)
0
2
4
6
8
10
Time (s)

Fig.3(a)

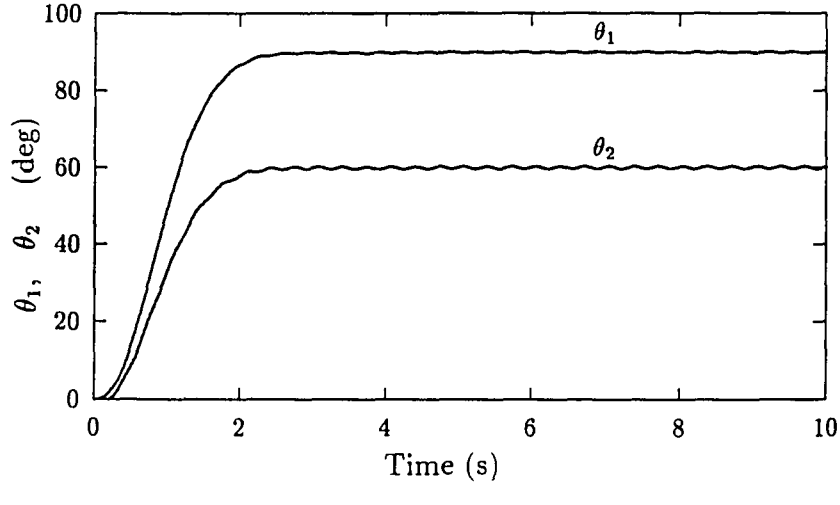
θ_1
θ_2
100
80
60
40
20
0
θ_1, θ_2 (deg)
0
2
4
6
8
10
Time (s)

Fig.3(b)

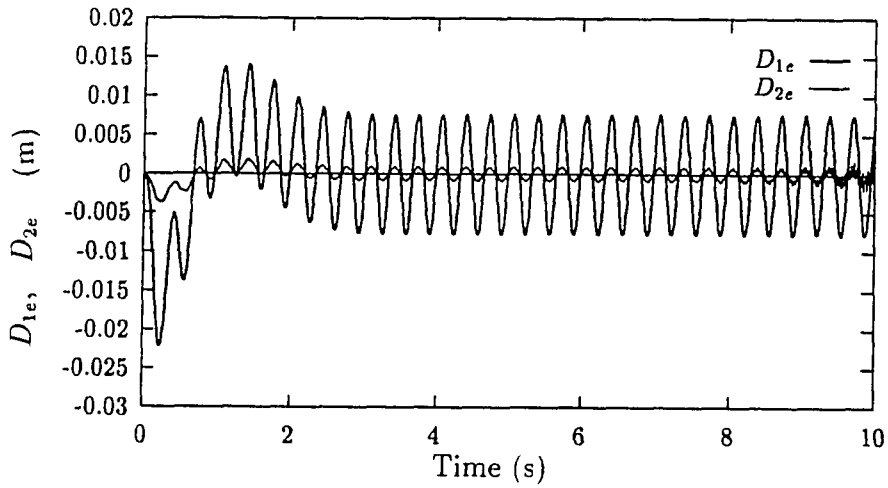
0.02
0.015
0.01
0.005
0
-0.005
-0.01
-0.015
-0.02
-0.025
-0.03
D_{1e}, D_{2e} (m)
D_{1e}
D_{2e}
0
2
4
6
8
10
Time (s)

Fig.3(c)

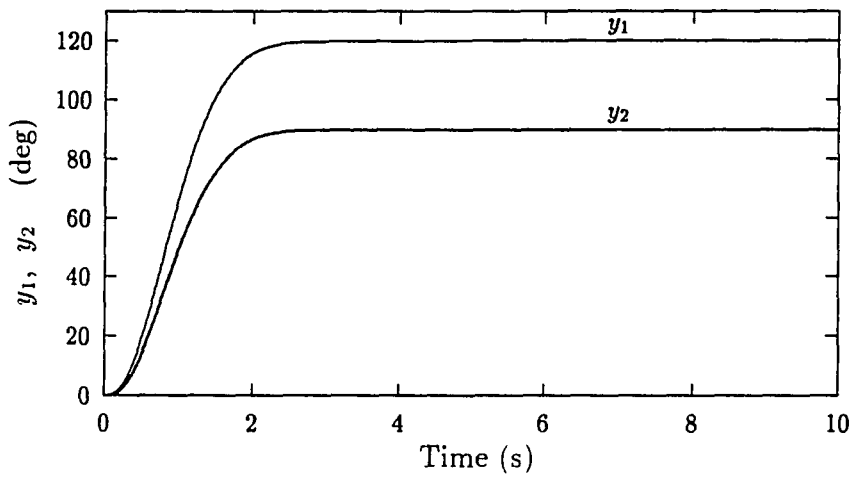
120
100
80
60
40
20
0
y_1, y_2 (deg)
y_1
y_2
0
2
4
6
8
10
Time (s)

Fig.4(a)

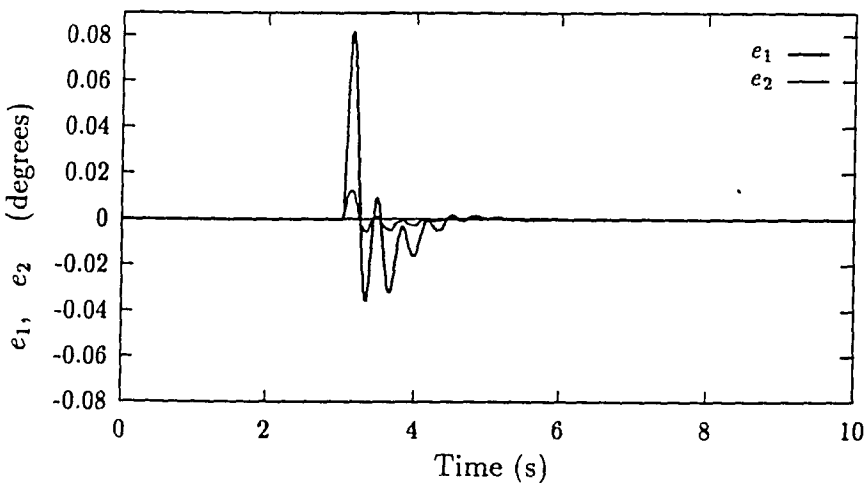
0.08
0.06
0.04
0.02
0
-0.02
-0.04
-0.06
-0.08
e_1, e_2 (degrees)
0
2
4
6
8
10
Time (s)
e_1
e_2

Fig.4(b)

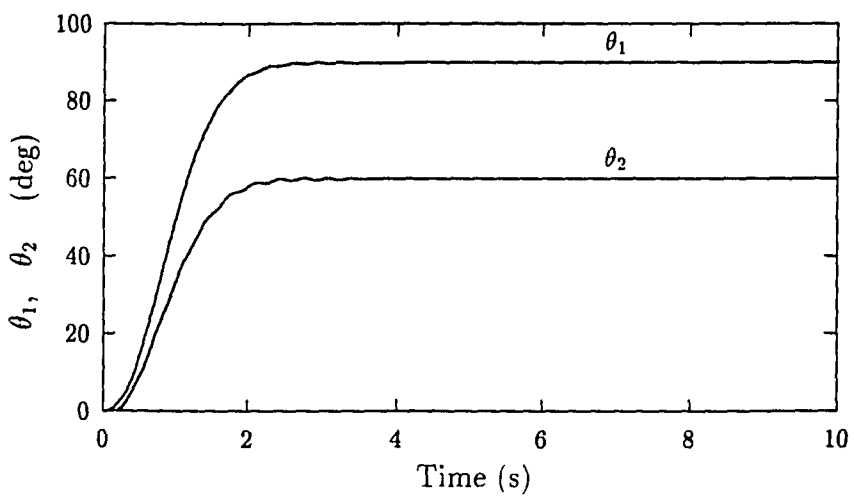
100
80
60
40
20
0
θ_1, θ_2 (deg)
0
2
4
6
8
10
Time (s)
θ_1
θ_2

Fig.4(c)

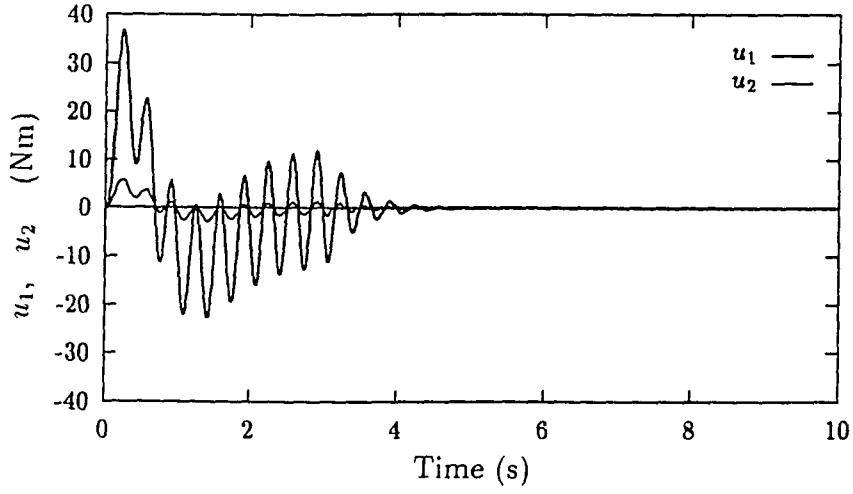
40
30
20
10
0
-10
-20
-30
-40
0
2
4
6
8
10
Time (s)
u_1, u_2 (Nm)
u_1
u_2

Fig.4(d)

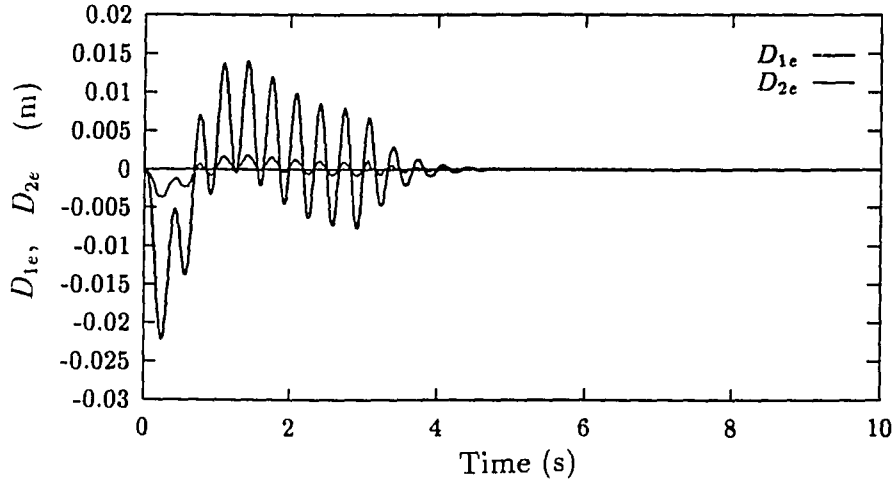
0.02
0.015
0.01
0.005
0
-0.005
-0.01
-0.015
-0.02
-0.025
-0.03
0
2
4
6
8
10
Time (s)
D_{1e}, D_{2e} (m)
D_{1e}
D_{2e}

Fig.4(e)

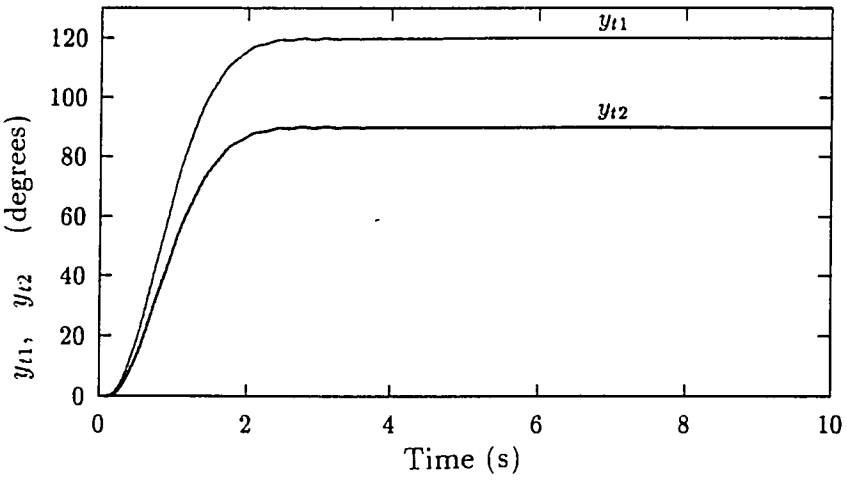
y_{t1}
y_{t2}
120
100
80
60
40
20
0
y_{t1}, y_{t2} (degrees)
0
2
4
6
8
10
Time (s)

Fig.4(f)

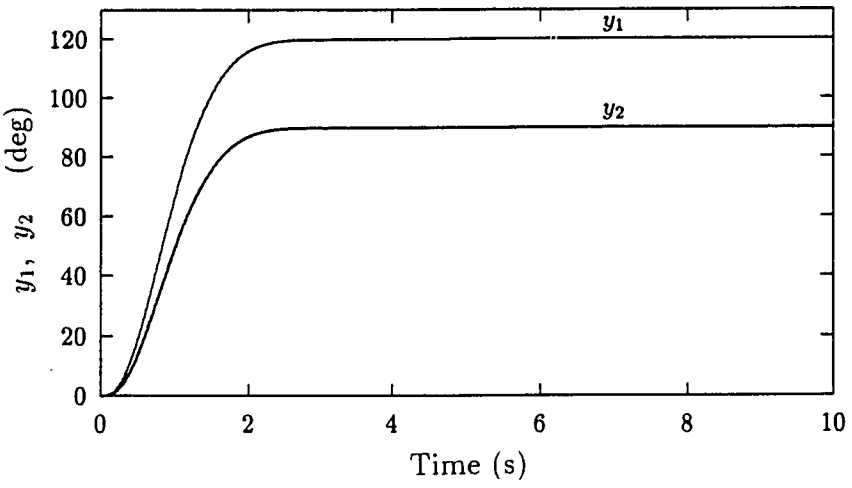
y_1
y_2
120
100
80
60
40
20
0
y_1, y_2 (deg)
0
2
4
6
8
10
Time (s)

Fig.5(a)

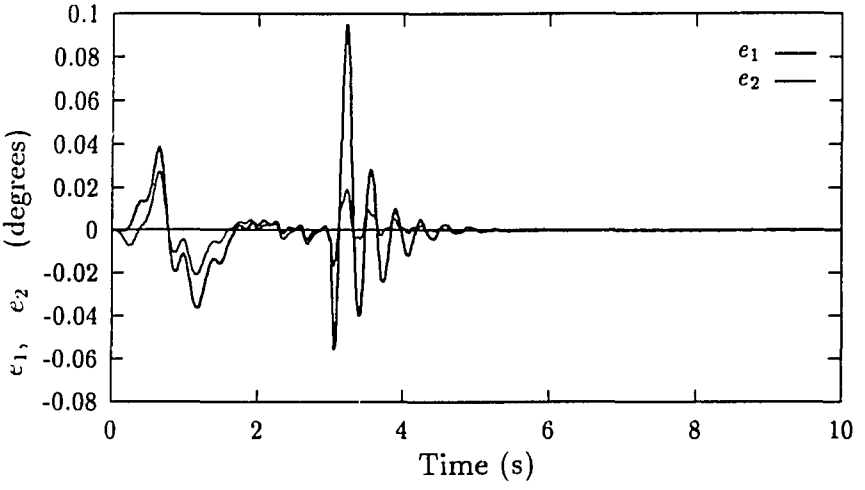
0.1
0.08
0.06
0.04
0.02
0
-0.02
-0.04
-0.06
-0.08
e_1, e_2 (degrees)
e_1
e_2
0
2
4
6
8
10
Time (s)

Fig.5(b)

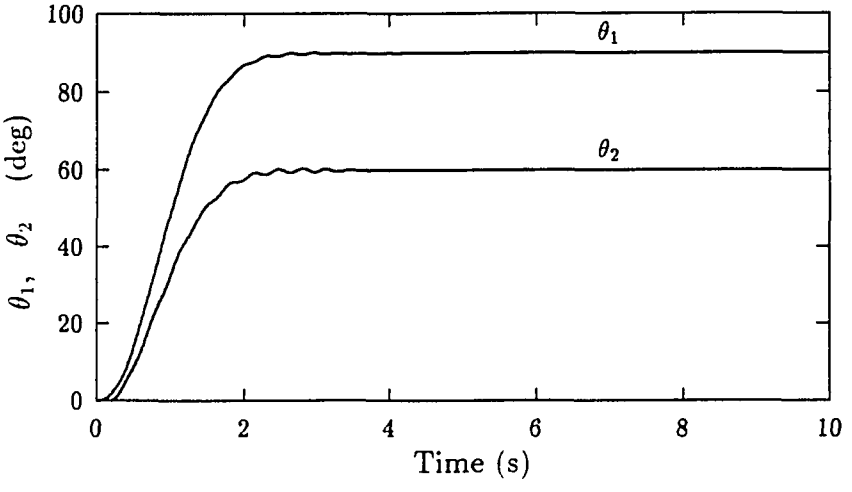
100
80
60
40
20
0
θ_1, θ_2 (deg)
θ_1
θ_2
0
2
4
6
8
10
Time (s)

Fig.5(c)

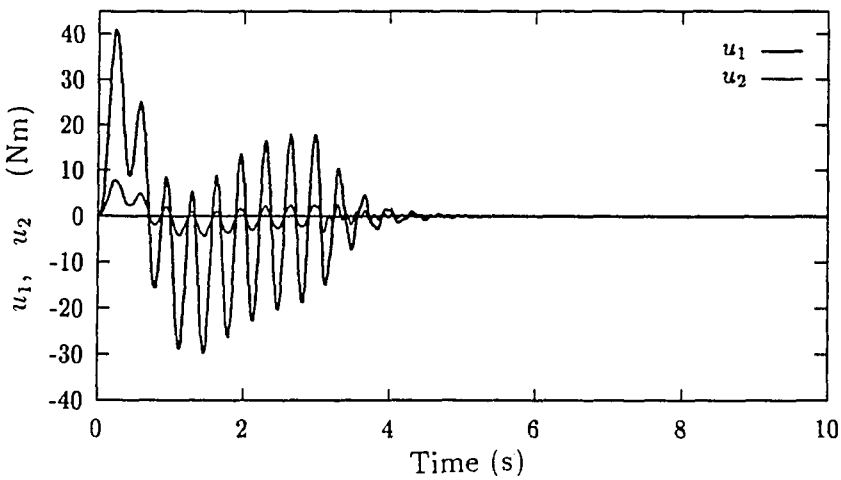
40
30
20
10
0
-10
-20
-30
-40
0
2
4
6
8
10
Time (s)
u_1, u_2 (Nm)
u_1
u_2

Fig.5(d)

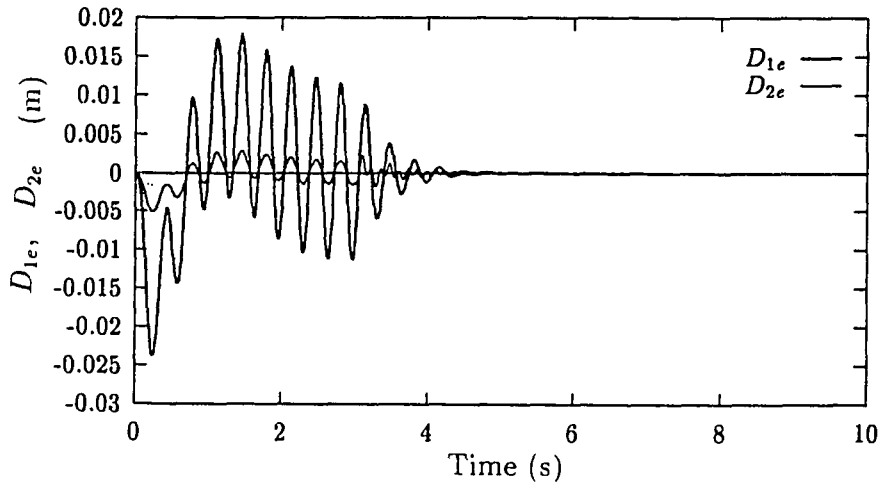
0.02
0.015
0.01
0.005
0
-0.005
-0.01
-0.015
-0.02
-0.025
-0.03
0
2
4
6
8
10
Time (s)
D_{1e}, D_{2e} (m)
D_{1e}
D_{2e}

Fig.5(e)

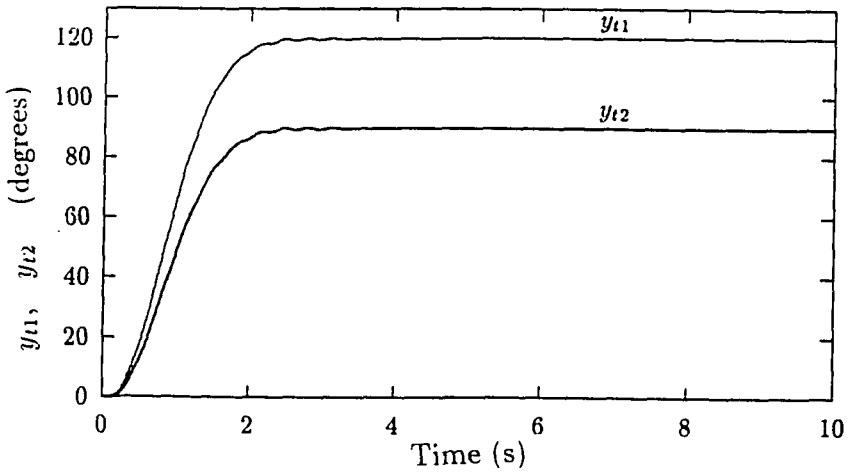
y_{t1}
y_{t2}
120
100
80
60
40
20
0
y_{t1}, y_{t2} (degrees)
0
2
4
6
8
10
Time (s)

Fig.5(f)

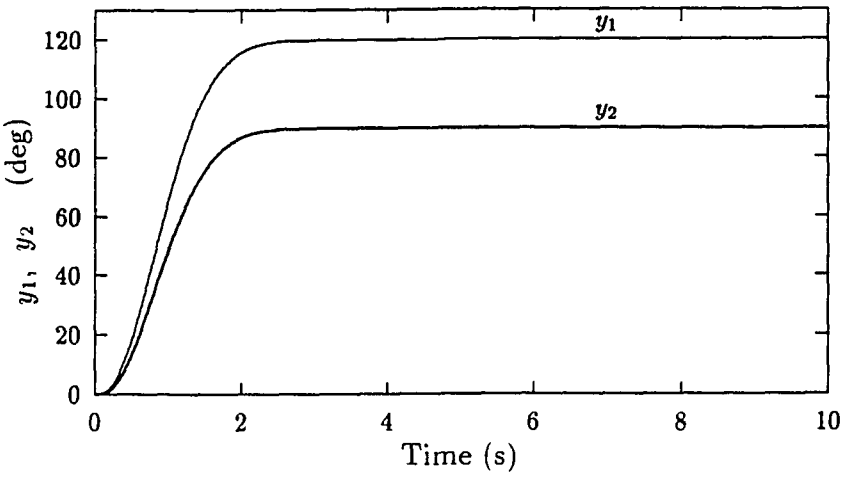
y_1
y_2
120
100
80
60
40
20
0
y_1, y_2 (deg)
0
2
4
6
8
10
Time (s)

Fig.6(a)

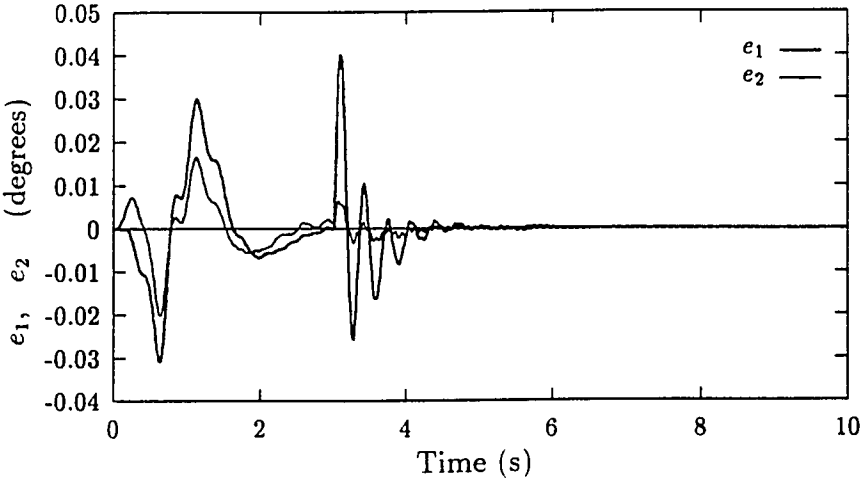
0.05
0.04
0.03
0.02
0.01
0
-0.01
-0.02
-0.03
-0.04
e_1, e_2 (degrees)
e_1
e_2
0
2
4
6
8
10
Time (s)

Fig.6(b)

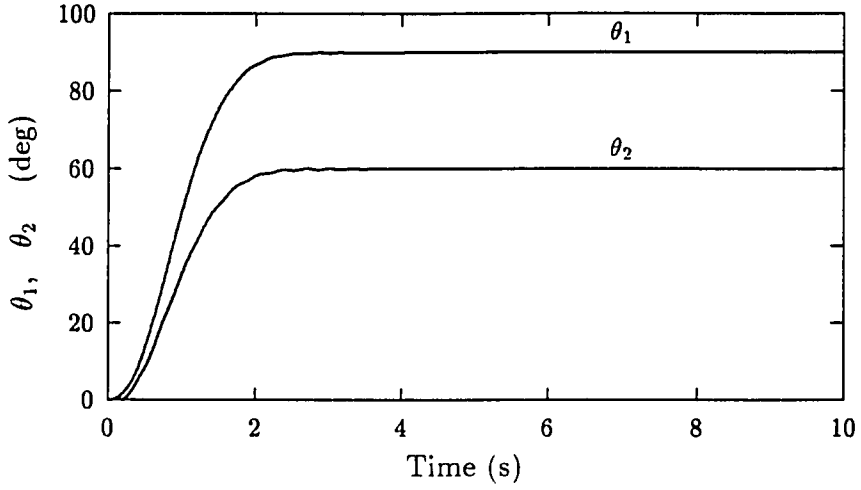
100
80
60
40
20
0
θ_1, θ_2 (deg)
θ_1
θ_2
0
2
4
6
8
10
Time (s)

Fig.6(c)

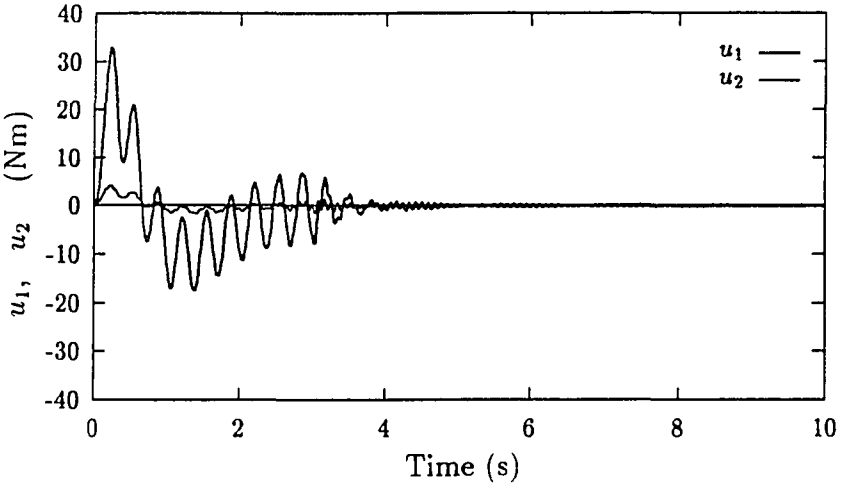
40
30
20
10
0
-10
-20
-30
-40
0
2
4
6
8
10
Time (s)
u_1, u_2 (Nm)
u_1
u_2

Fig.6(d)

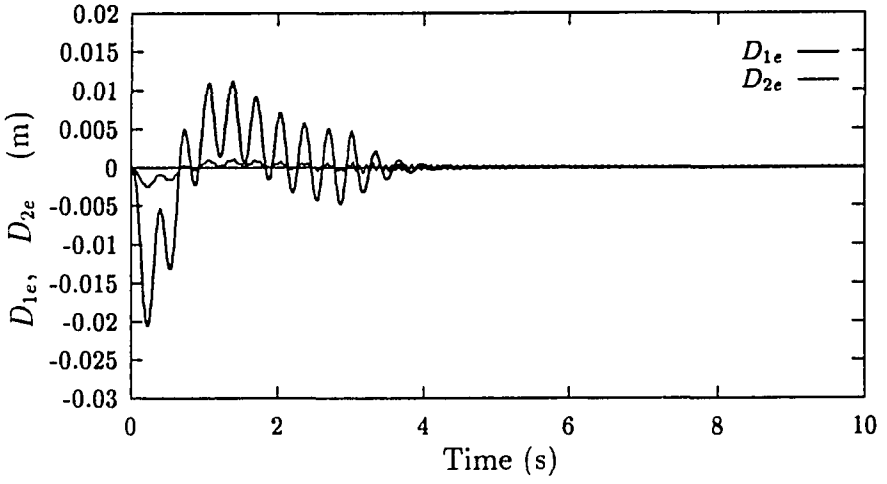
0.02
0.015
0.01
0.005
0
-0.005
-0.01
-0.015
-0.02
-0.025
-0.03
0
2
4
6
8
10
Time (s)
D_{1e}, D_{2e} (m)
D_{1e}
D_{2e}

Fig.6(e)

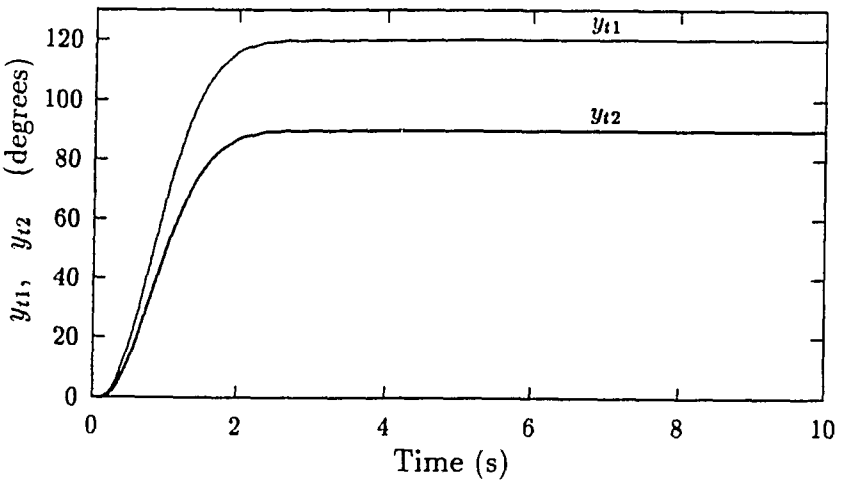
y_{t1}
y_{t2}
120
100
80
60
40
20
0
y_{t1}, y_{t2} (degrees)
0
2
4
6
8
10
Time (s)

Fig.6(f)

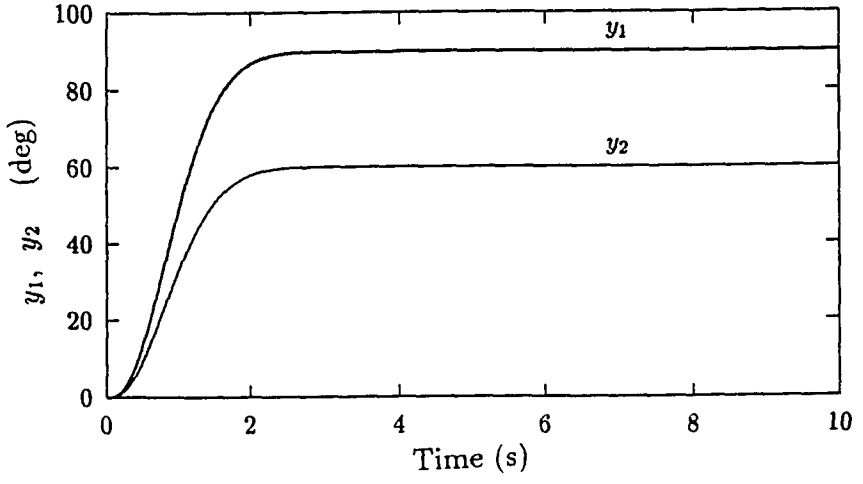
y_1
y_2
100
80
60
40
20
0
y_1, y_2 (deg)
0
2
4
6
8
10
Time (s)

Fig.7(a)

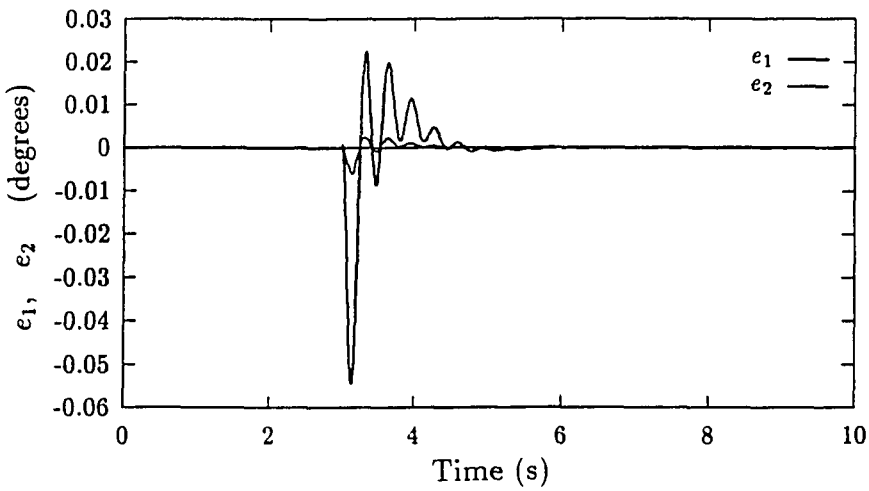
0.03
0.02
0.01
0
-0.01
-0.02
-0.03
-0.04
-0.05
-0.06
e_1, e_2 (degrees)
e_1
e_2
0
2
4
6
8
10
Time (s)

Fig.7(b)

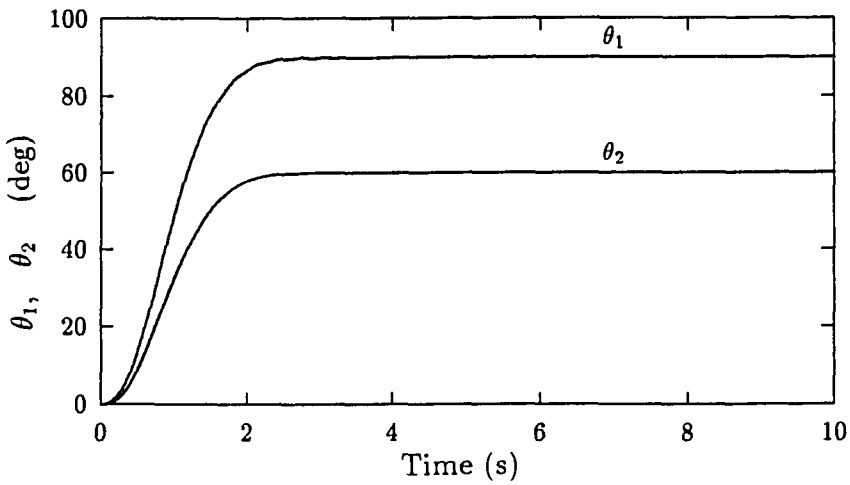
100
80
60
40
20
0
θ_1, θ_2 (deg)
θ_1
θ_2
0
2
4
6
8
10
Time (s)

Fig.7(c)

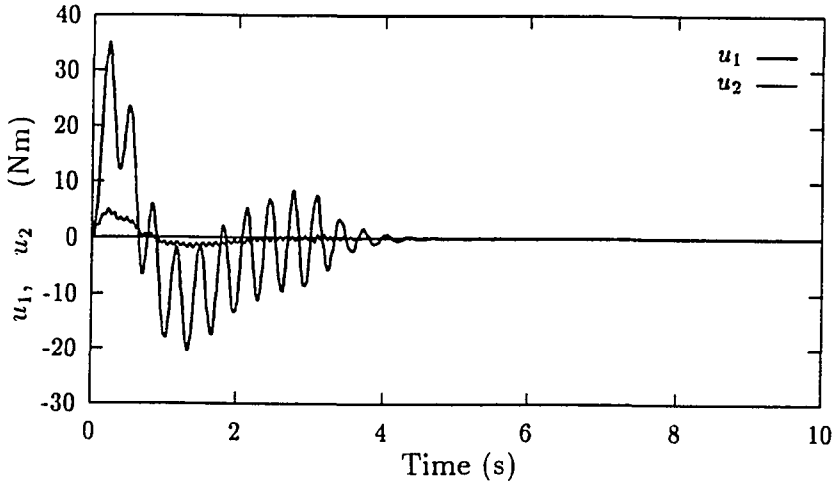
40
30
20
10
0
-10
-20
-30
u_1, u_2 (Nm)
0
2
4
6
8
10
Time (s)
u_1
u_2

Fig.7(d)

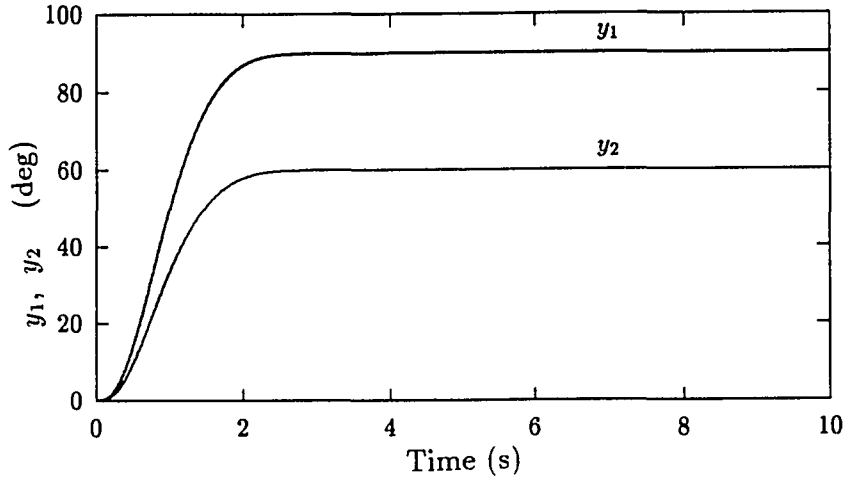
100
80
60
40
20
0
y_1, y_2 (deg)
0
2
4
6
8
10
Time (s)
y_1
y_2

Fig.8(a)

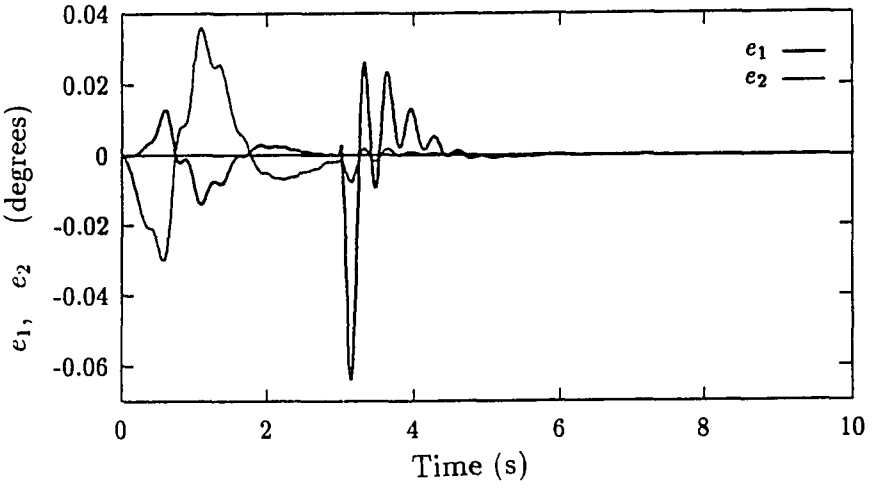
0.04
0.02
0
-0.02
-0.04
-0.06
e_1, e_2 (degrees)
e_1
e_2
0
2
4
6
8
10
Time (s)

Fig.8(b)

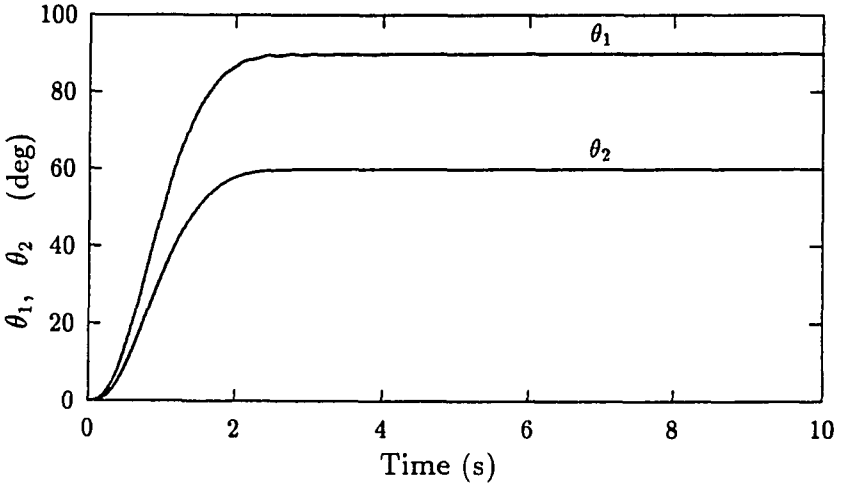
100
80
60
40
20
0
θ_1, θ_2 (deg)
θ_1
θ_2
0
2
4
6
8
10
Time (s)

Fig.8(c)

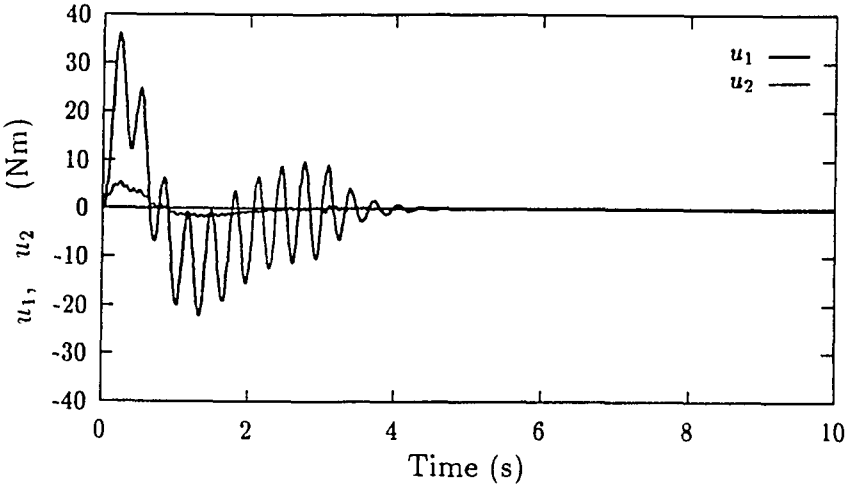
40
30
20
10
0
-10
-20
-30
-40
u_1, u_2 (Nm)
0
2
4
6
8
10
Time (s)
u_1
u_2

Fig.8(d)

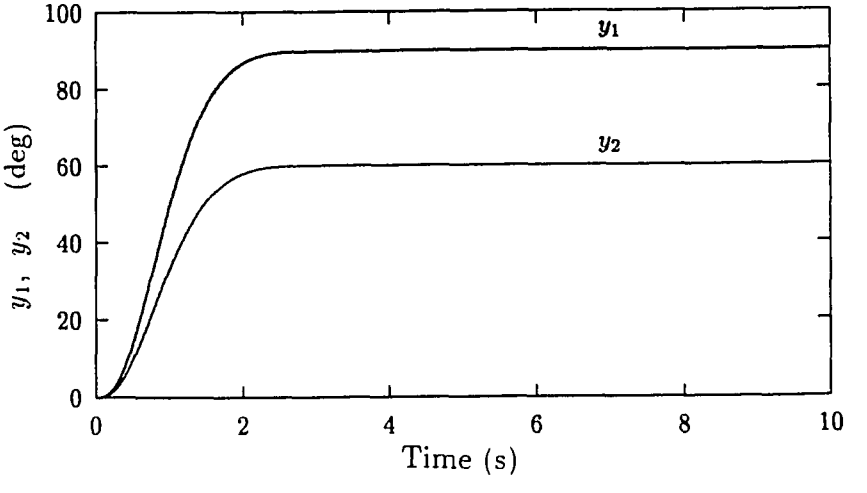
100
80
60
40
20
0
y_1, y_2 (deg)
0
2
4
6
8
10
Time (s)
y_1
y_2

Fig.9(a)

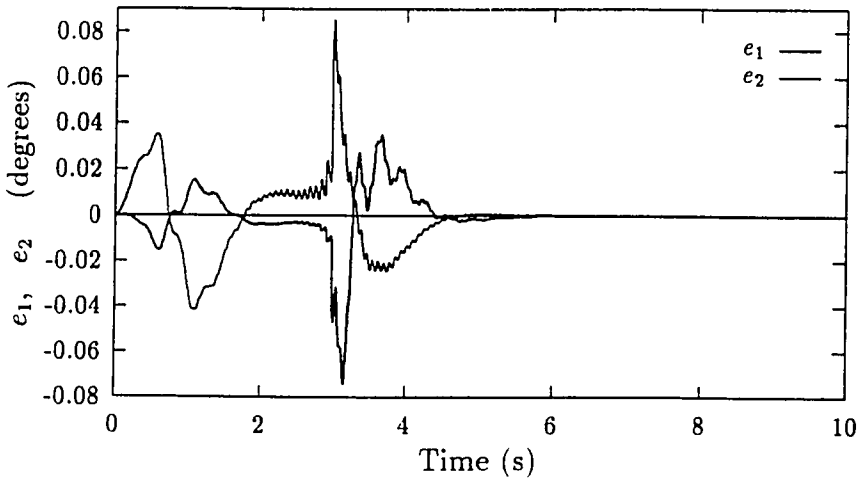
0.08
0.06
0.04
0.02
0
-0.02
-0.04
-0.06
-0.08
e_1, e_2 (degrees)
e_1
e_2
0
2
4
6
8
10
Time (s)

Fig.9(b)

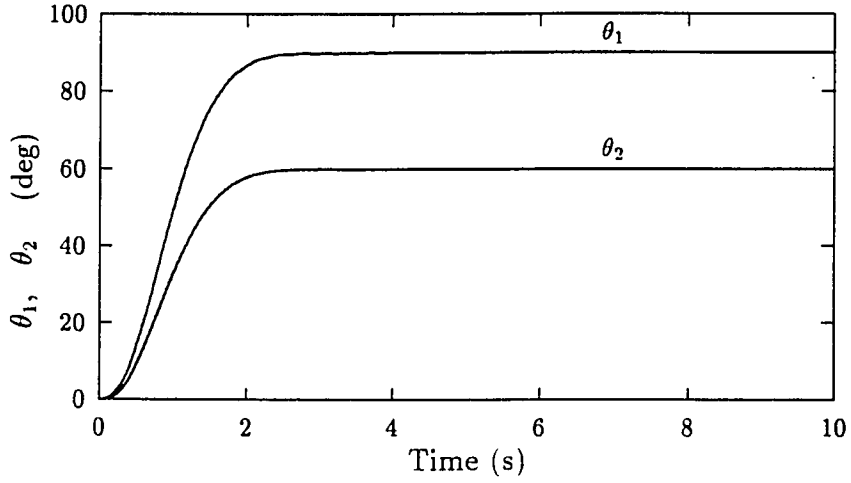
100
80
60
40
20
0
θ_1, θ_2 (deg)
θ_1
θ_2
0
2
4
6
8
10
Time (s)

Fig.9(c)

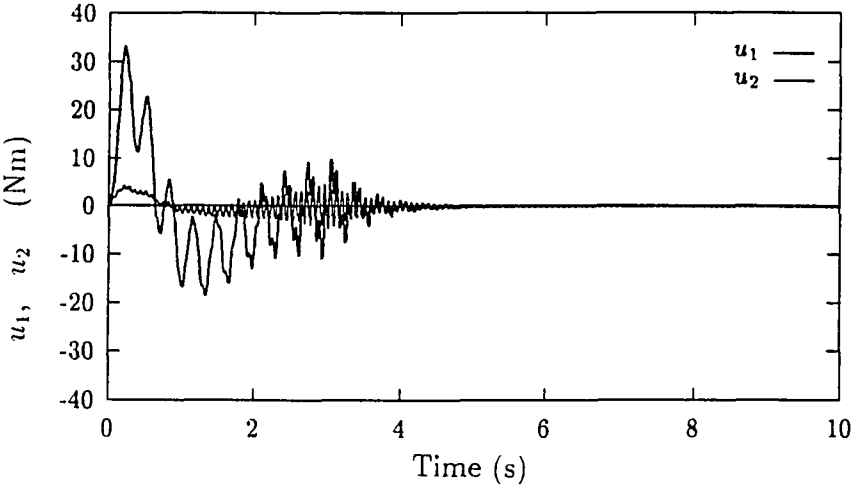

Fig.9(d)

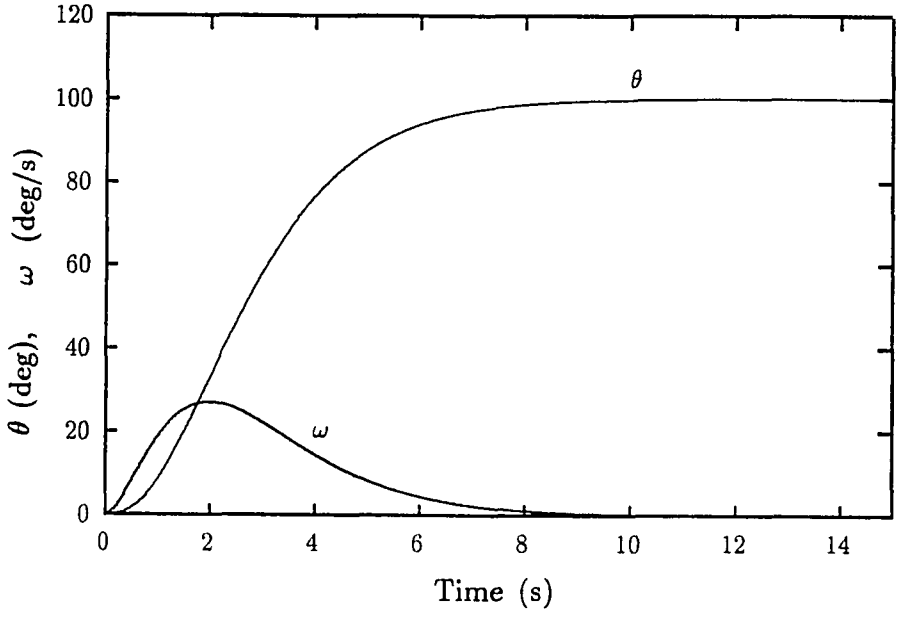

Fig.10(a)

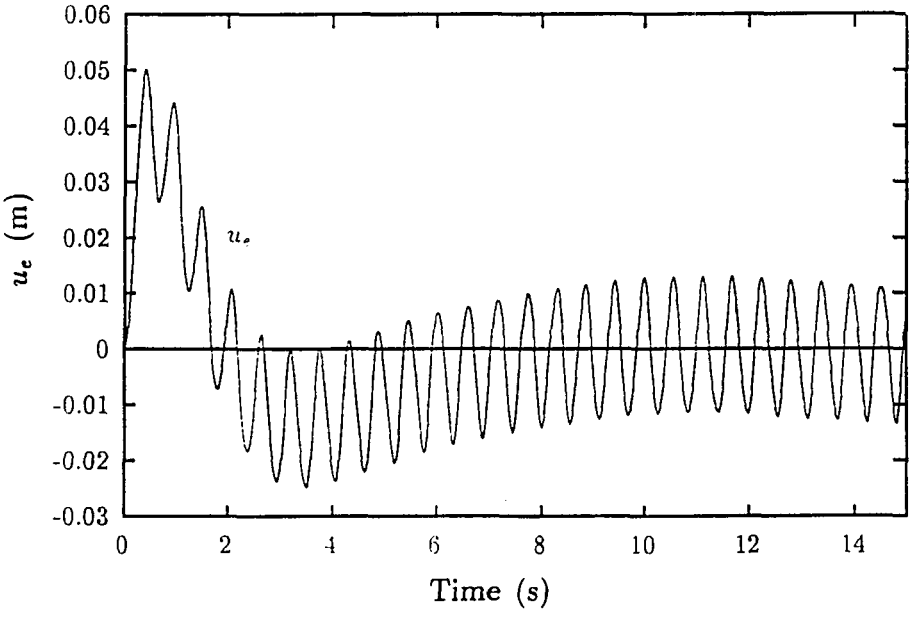

Fig.10(b)

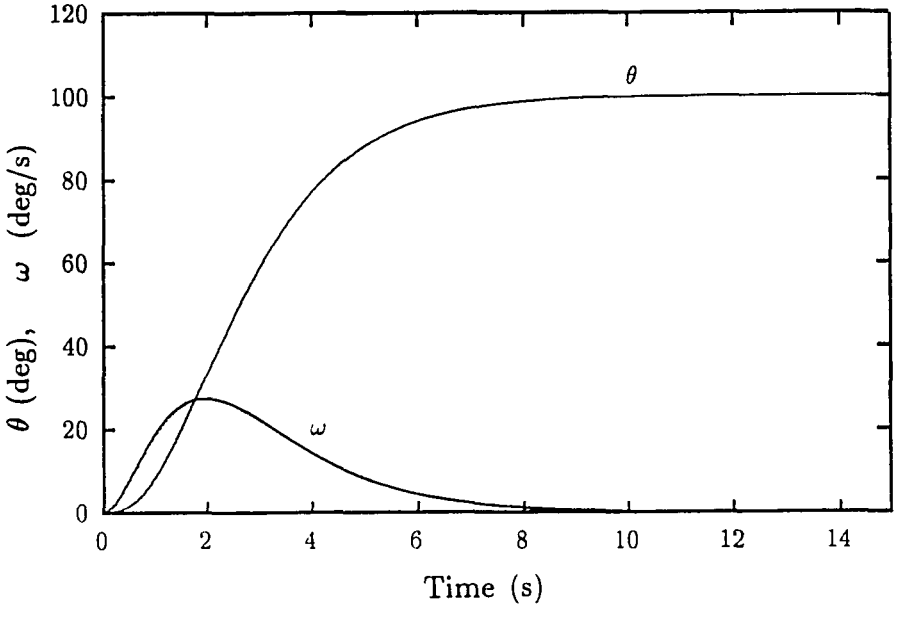

Fig.11(a)

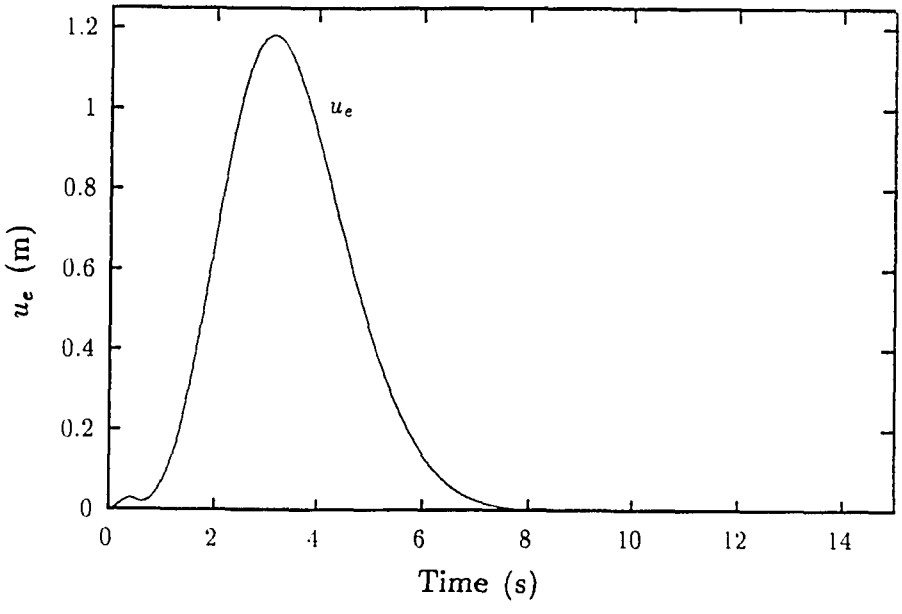

Fig.11(b)

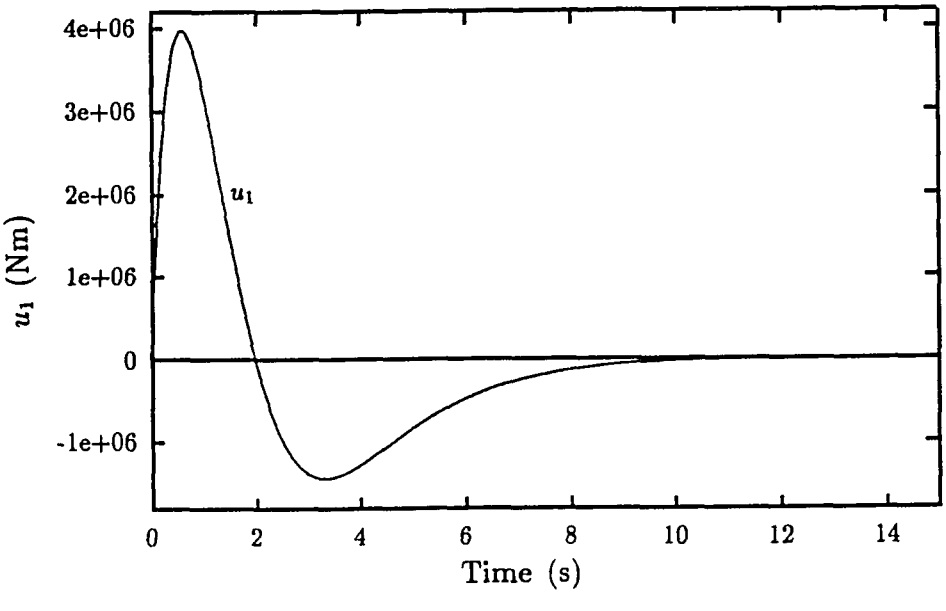

Fig.11(c)

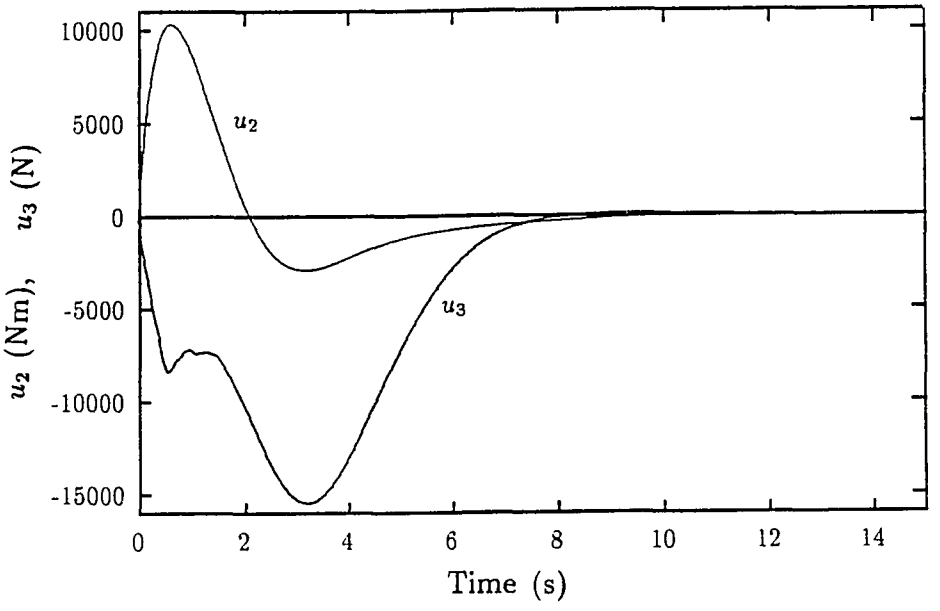

Fig.11(d)

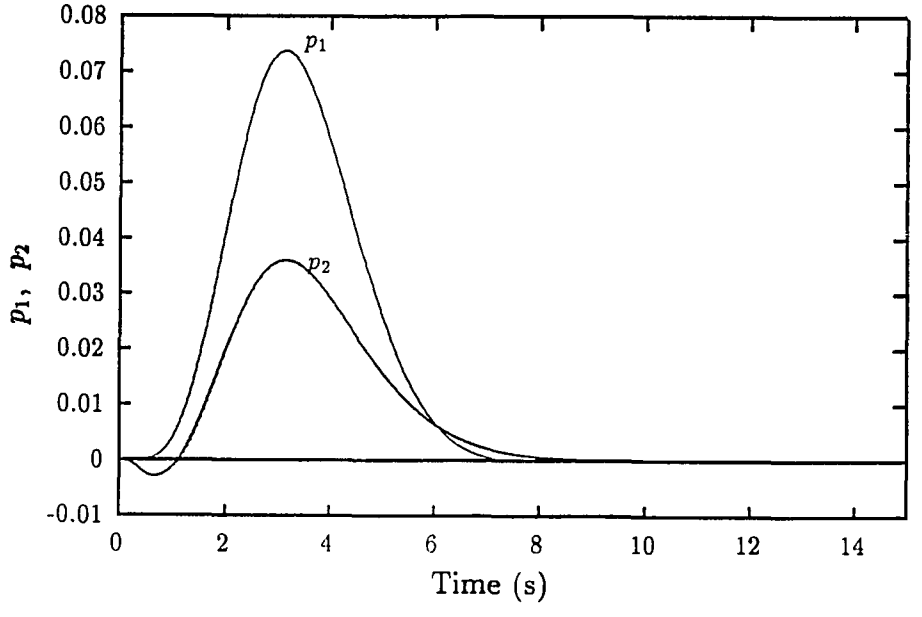

Fig.11(e)

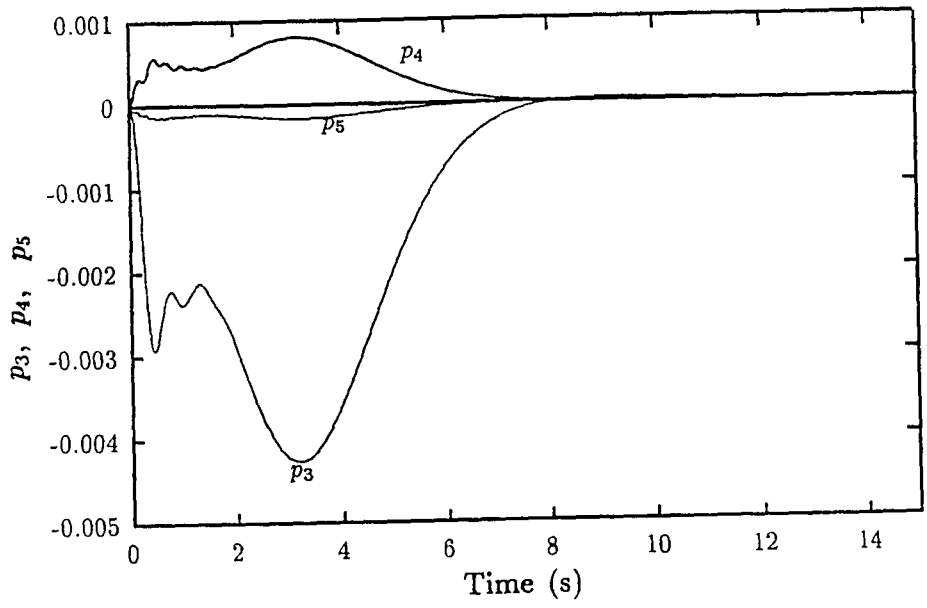

Fig.11(f)

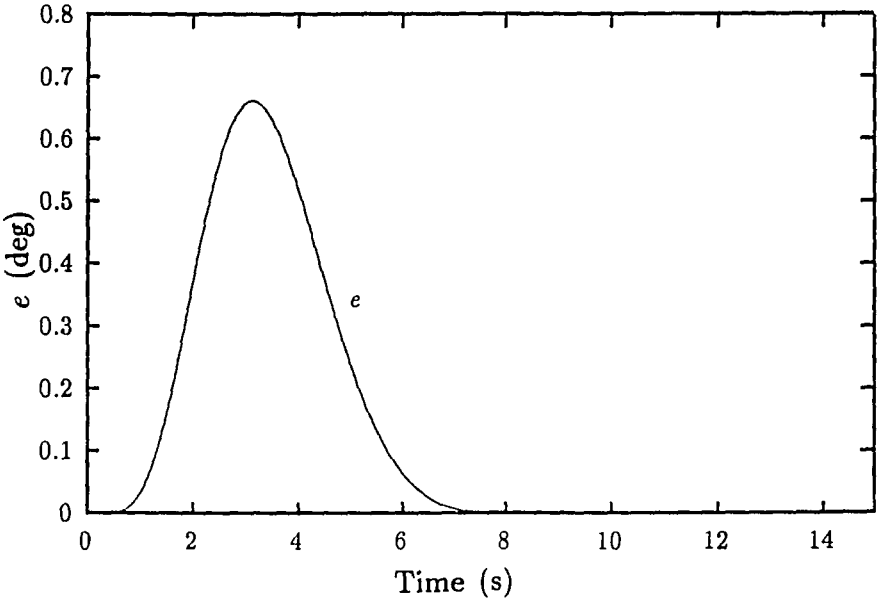

Fig.11(g)

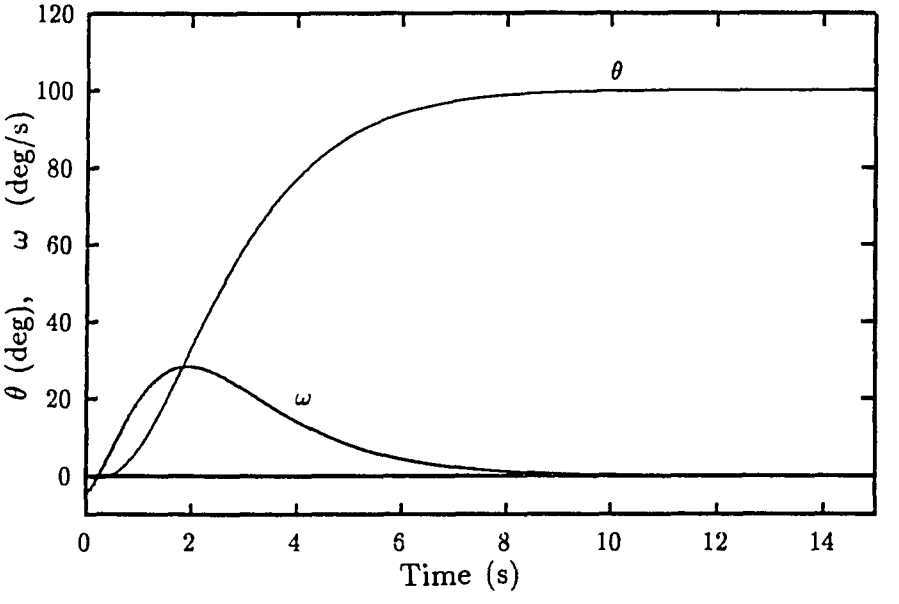

Fig.12(a)

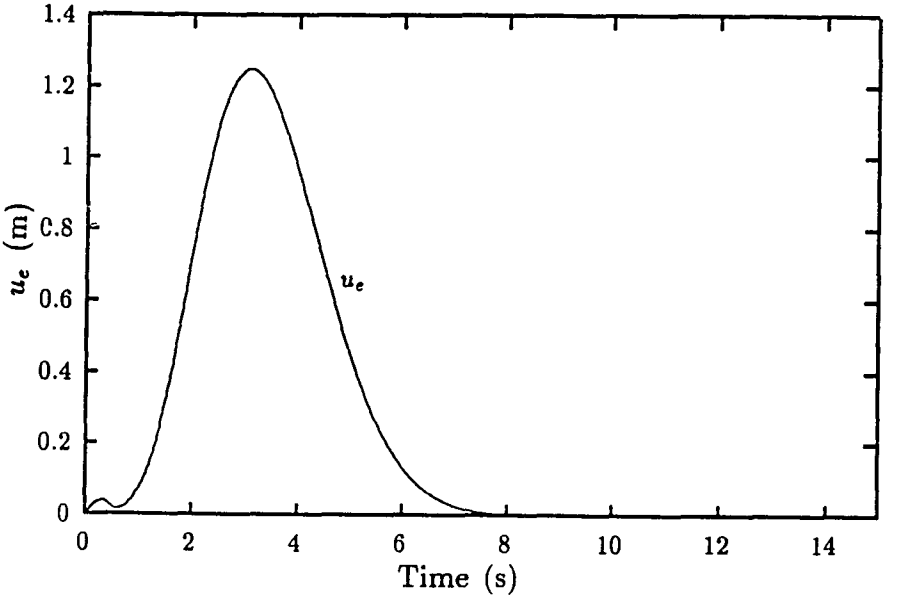

Fig.12(b)

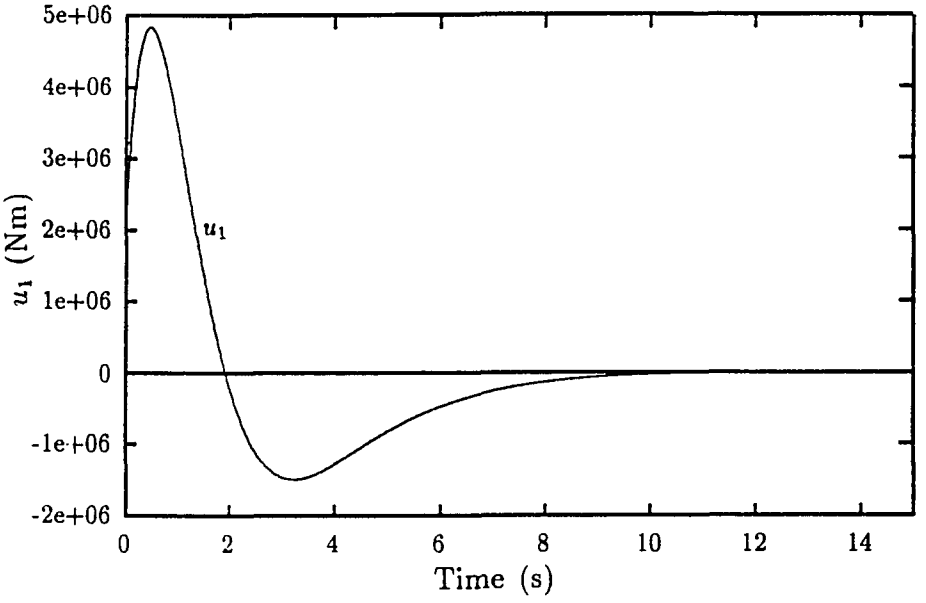

Fig.12(c)

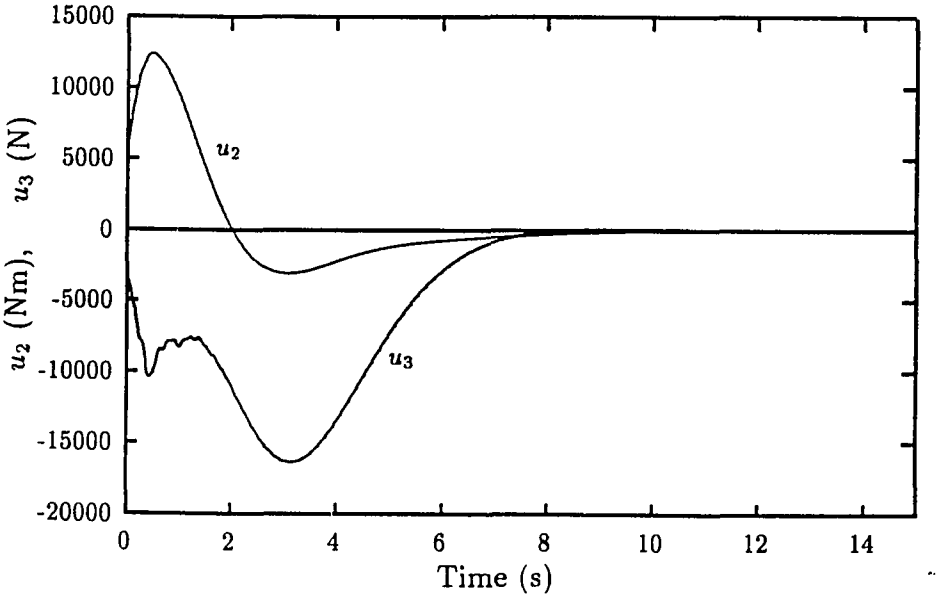

Fig.12(d)

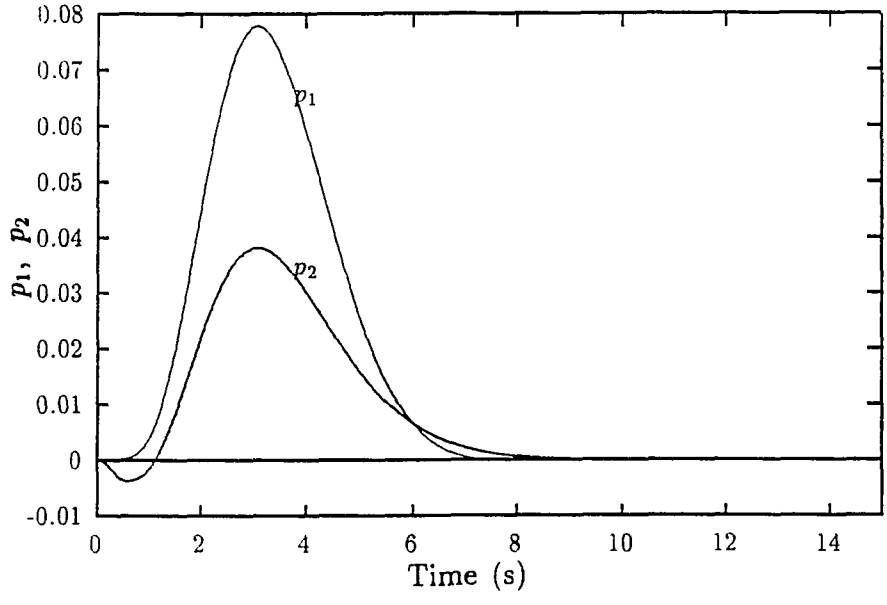

Fig.12(e)

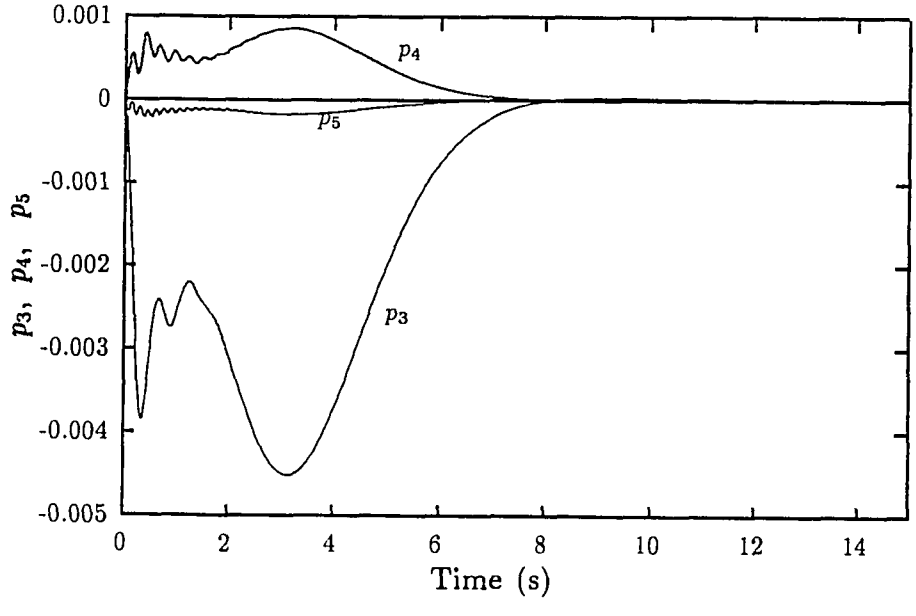

Fig.12(f)

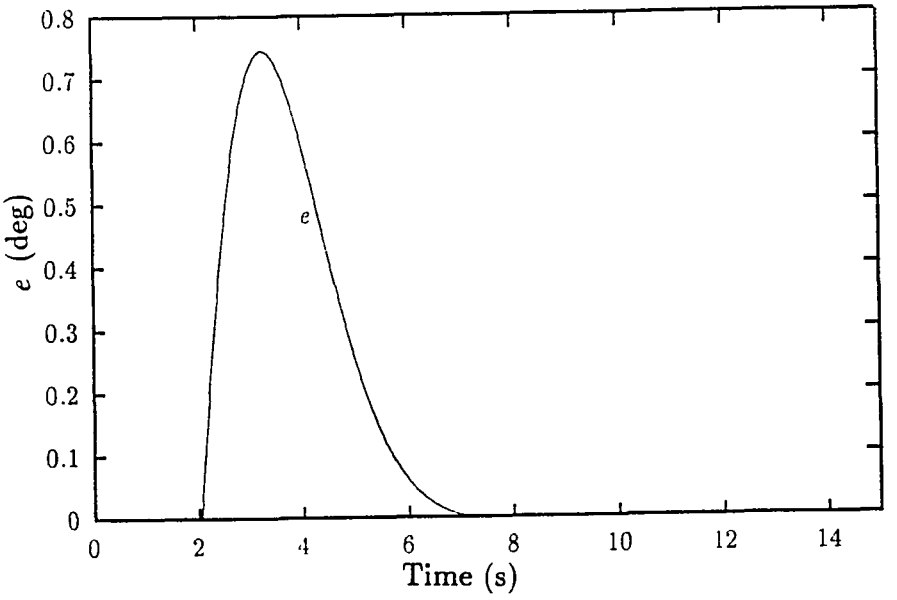

Fig.12(g)

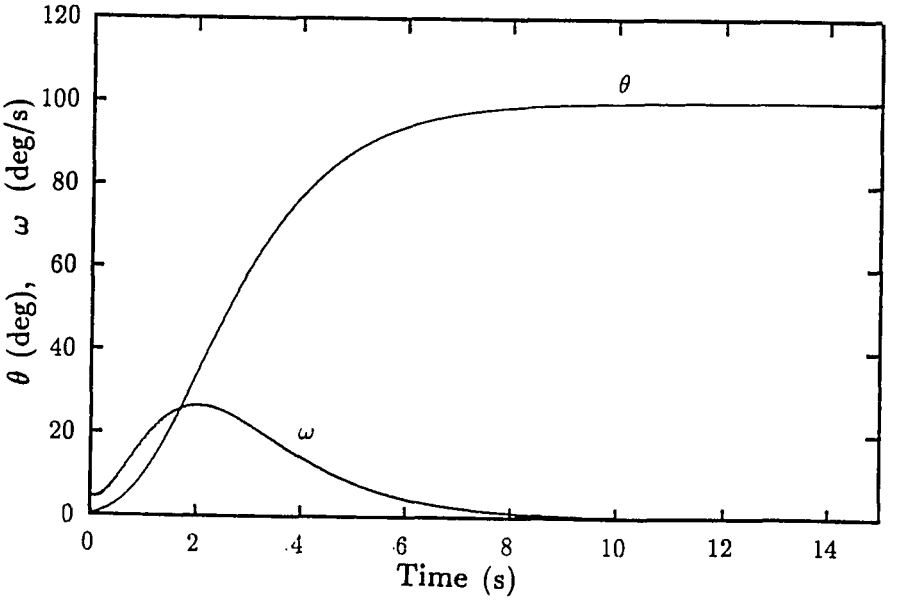

Fig.13(a)

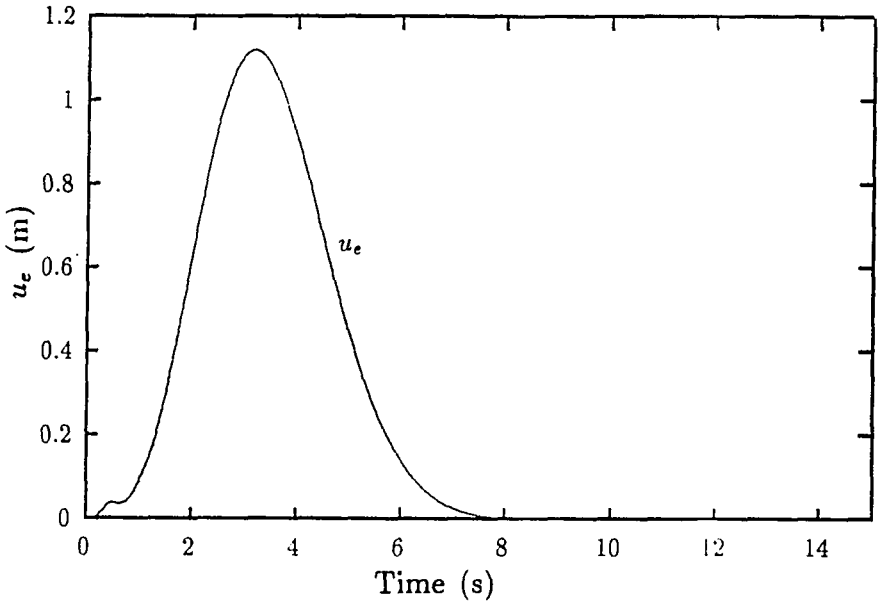

Fig.13(b)

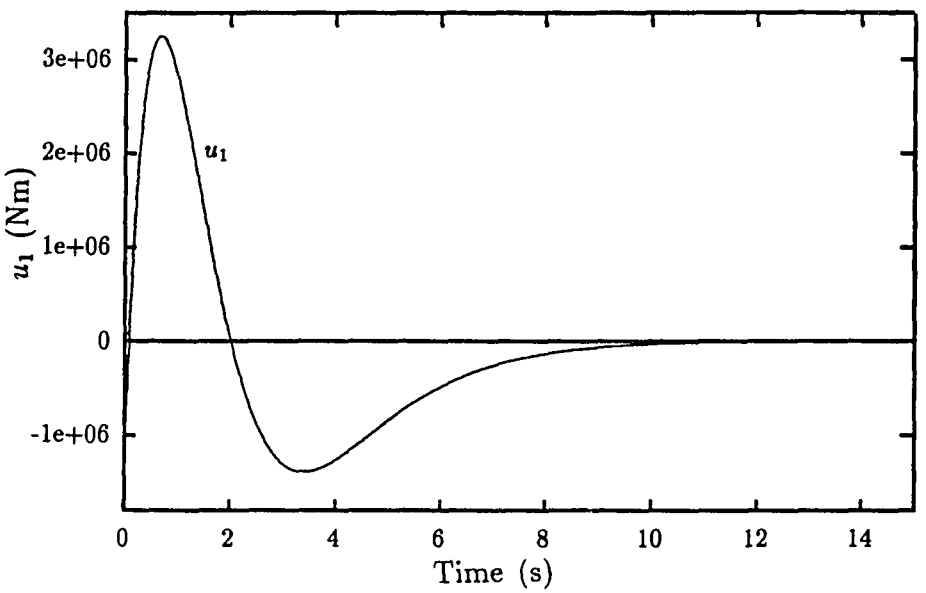

Fig.13(c)

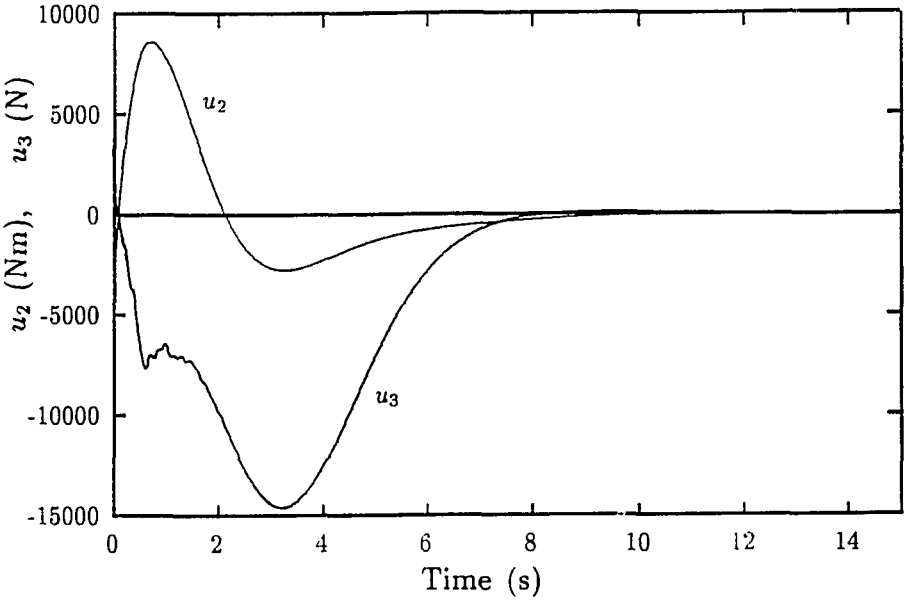

Fig.13(d)

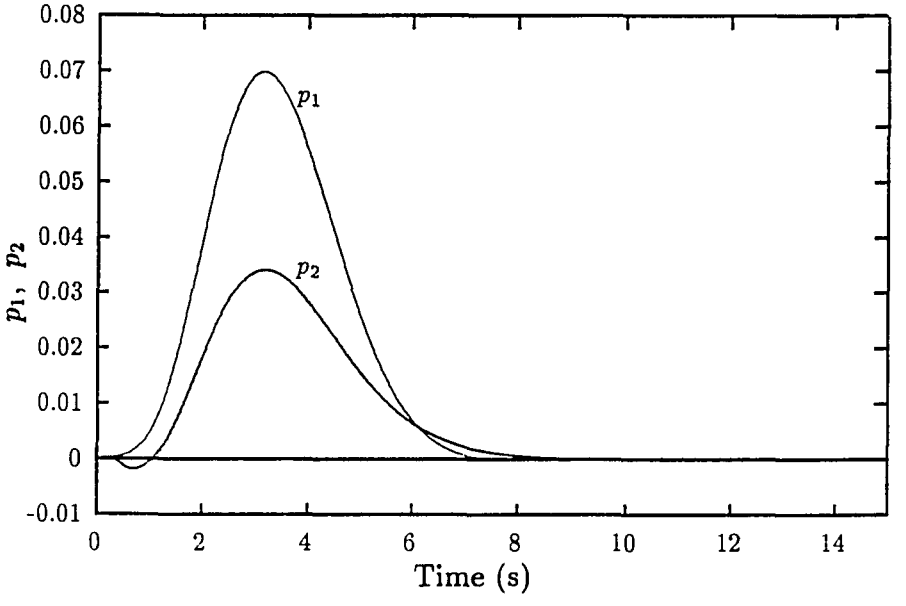

Fig.13(e)

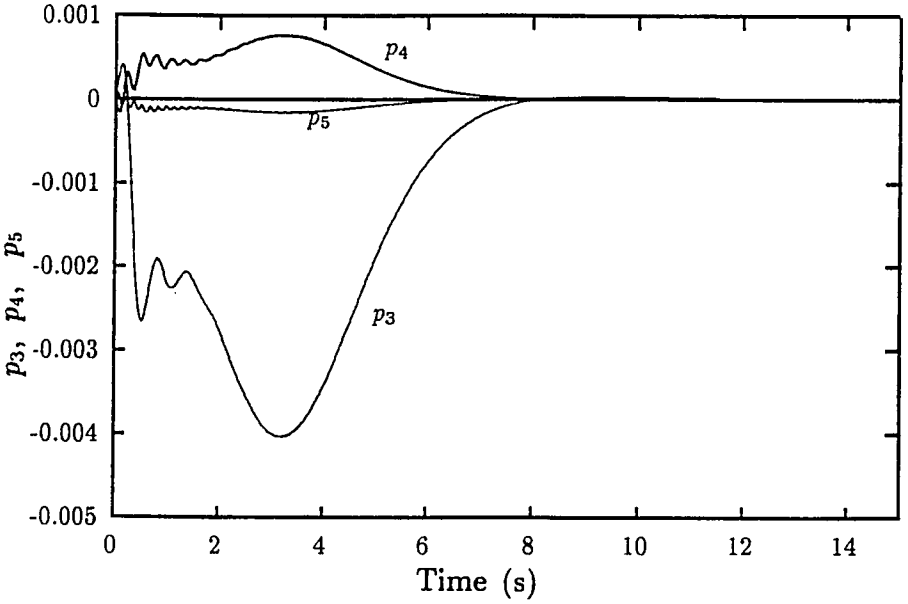

Fig.13(f)

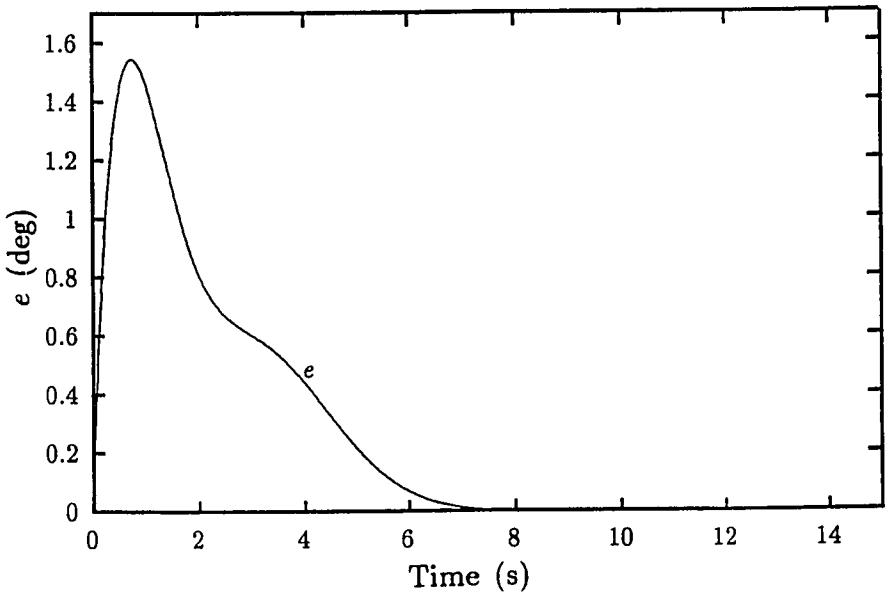

Fig.13(g)

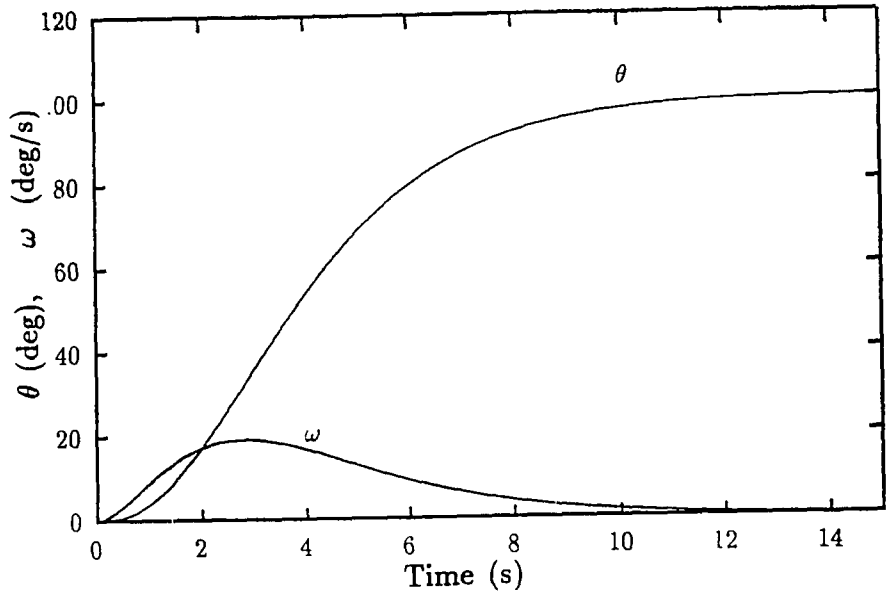

Fig.14(a)

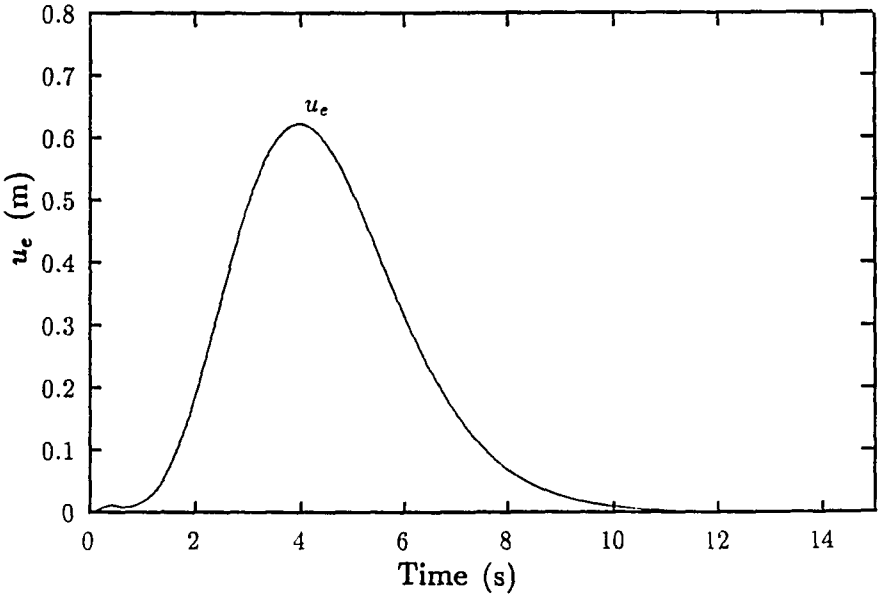

Fig.14(b)

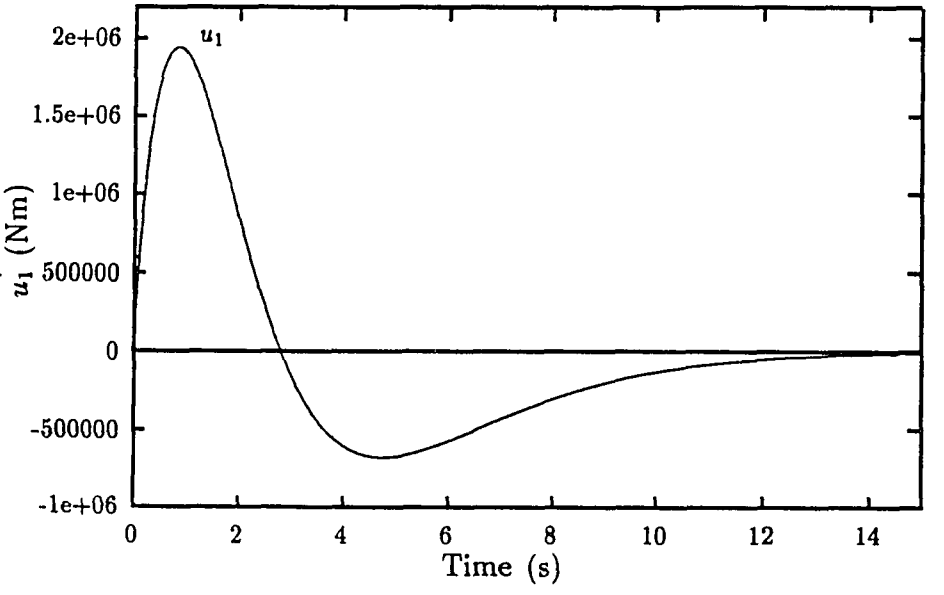

Fig.14(c)

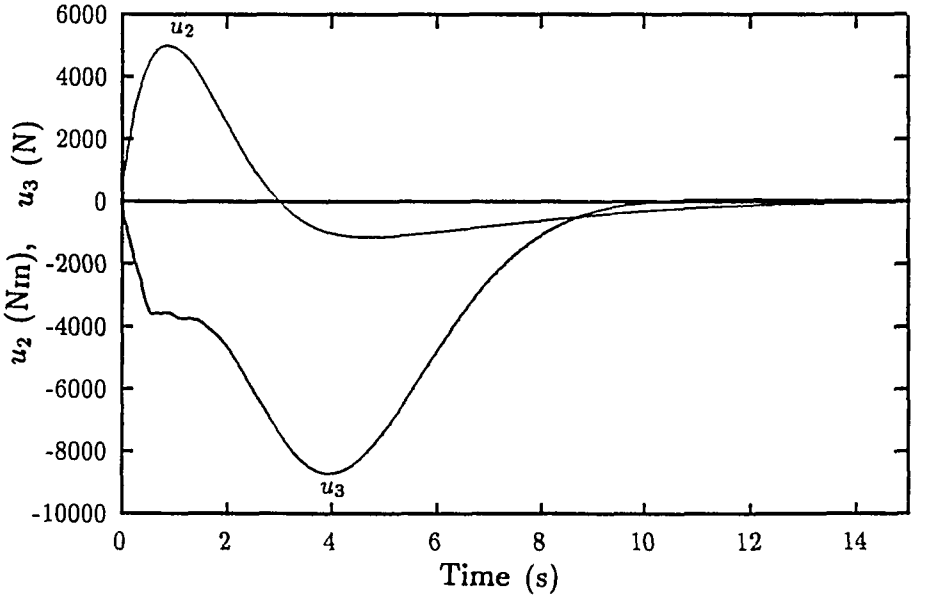

Fig.14(d)

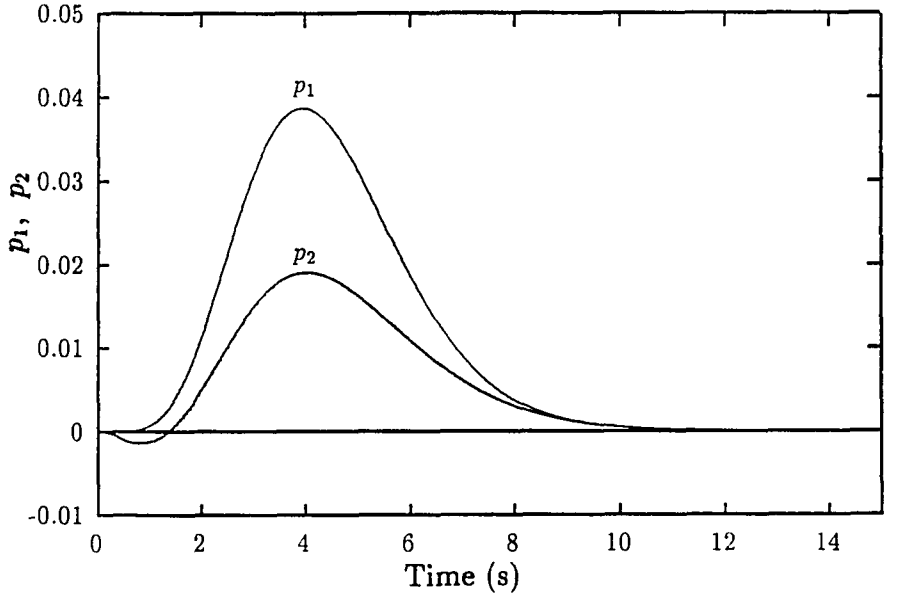

Fig.14(e)

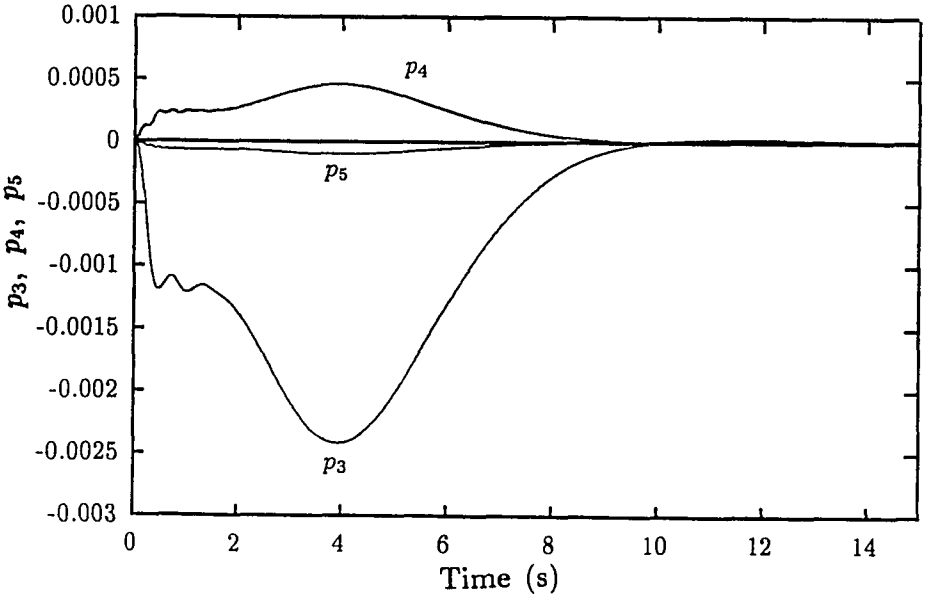

Fig.14(f)

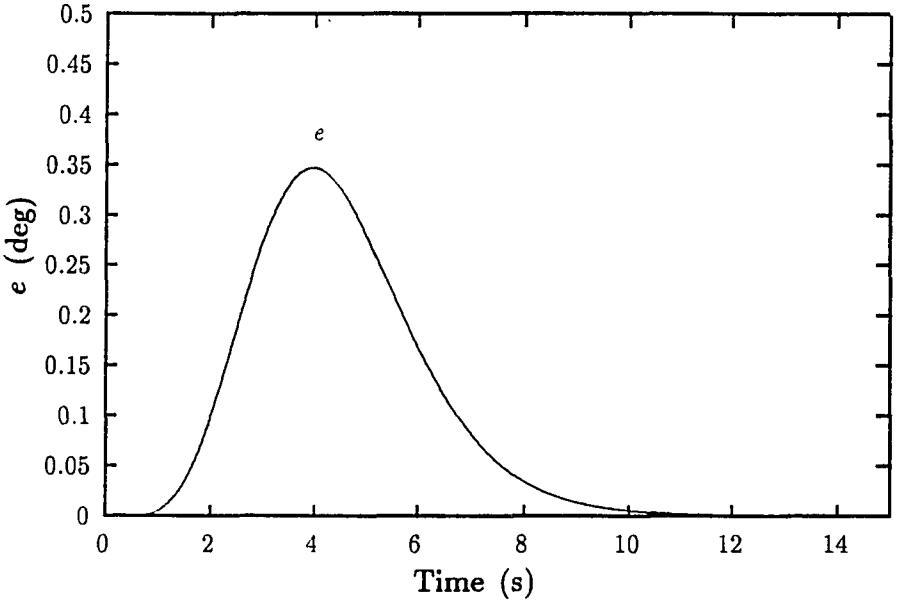

Fig.14(g)

Bibliography

1. A. De. Luca, P. Lucibello and G. Ulivi, Inversion techniques for trajectory control of flexible robot arms, *J.Robotic Systems.*, Vol.6, no.4, pp-25-344 (1989).

2. A. De. Luca, and B. Siciliano, Trajectory control of a nonlinear one-link flexible arm, *Int. J. of Control.*, Vol.50, no.5, pp. 1699-1715 (1989).

3. P. Lucibello, Nonlinear regulation with Internal stability of a two-link flexible robotic arm, *Proc. IEEE Conf. on Decision and Control, Tampa, FL.*, pp.1645-1650 (1989).

4. S. K. Madhavan, and S. N. Singh, Inverse Trajectory control and Zero dynamic sensitivity of an elastic manipulator,*International Journal of Robotics and Automation.*, vol. 6, no. 4, pp. 179-192 (1991).

5. D. Wang, and M. Vidyasagar, Transfer functions for a single flexible link, *IEEE International Conference on Robotics and Automation, Scottsdale, Arizona.*, pp. 1042-1047, May 1989.

6. R. H. Canon Jr., and E. Schmitz, Initial experiments on the end-point control of a one link flexible experimental manipulator, *Journal of Robotic Systems.*, vol. 3, pp. 62-75 (1984).

7. D. C. Nemir, A. J. Koivo, and R. L. Kashyap, Pseudolinks and the self-tuning control of a nonrigid link mechanism, *IEEE Transactions on Systems, Man and Cybernetics.*, vol. 18, pp. 40-48 (1988).

8. E. Bayo, A Finite-element approach to control the end-point motion of a single-link flexible robot, *J. of Robotic Systems.*, Vol.4, pp. 63-75 (1987).

9. E. Bayo, R. Movaghar, and M. Medus, Inverse Dynamics of Single- Link Flexible Robot. Analytical and Experimental Results, *IEEE International Conference on Robotics and Automation.*, Vol.3, No. 3, pp. 150-157(1988).

10. E. Bayo, P. Papadopoulos, J. Stubbe, and M. Serna,'Inverse Dynamics and Kinematics of Multi-Link Elastic Robots. An Iterative Frequency Domain Approach, *Journal Of Robotic Systems.*, vol. 8, No. 6, pp 49-62(1989).

11. S. K. Madhavan, and S. N. Singh, Variable Structure Trajectory Control of an Elastic Robotic Arm, *Journal Of Robotic Systems.*, 1993

12. J.-J.E. Slotine, and W. Li, *Applied Nonlinear Control*, Prentice Hall,1991

13. K. D. Young, Controller design for a manipulator using theory of variable structure systems, *IEEE Trans. on Systems, Man and Cybernetics.*, vol. SMC-8, No. 2, Feb. 1978.

14. B. E. Paden and S. S. Sastry, Calculus for computing Fillippov's Differential Inclusion with application to the Variable Structure Control of Robot Manipulator, *IEEE Trans. on Systems and Circuits.*, vol. 34, Jan. 1987, pp 73-82.

15. C. I. Byrnes and A. Isidori, Asymptotic stabilization of minimum phase nonlinear systems, *IEEE Trans. on Automatic Control.*, vol. 36, Oct. 1991, pp 1122-1137.

16. A. Isidori, *Nonlinear Control Systems*, 2nd ed., Springer-Verlag, New York, 1989.

17. O. Maizza-Neto, Modal analysis and control of flexible manipulator arms. Ph.D Thesis, Department of Mechanical Engineering, M.I.T., Cambridge(1973).

18. J. A. Breakwell, Optimal Feedback Control for Flexible Spacecraft. *J. Guidance Control Dynam* 4, 472-479(1981).

19. J. Ben-Asher, J. A. Burns and E. M. Cliff, Time Optimal Slewing of Flexible Spacecraft. *J. Guidance Control Dynam* **15**, 360-367(1992).

20. A. L. Hale and R. J. Lisowski, Characteristic Elastic Systems of Time-Limited Optimal Maneuvers. *J. Guidance Control Dynam* **8**, 628-636(1985).

21. G. Singh, P. T. Kabamba and N. H. McClamroch, Bang-Bang Control of Flexible Spacecraft Slewing Maneuvers: Guaranteed Terminal Pointing Accuracy. *J. Guidance Control Dynam* **13**, 376-379(1990).

22. S. B. Skaar, L. Tang and Y. Yalda-Mooshabad, On-Off Attitude Control of Flexible Satellites. *Journal of Guidance, Control, and Dynamics* **9**, 507-510 (1986)

23. R. M. Byers, S. R. Vadali and J. L. Junkins, Near-Minimum- Time Open-Loop Slewing Of Flexible Vehicles. *J. Guidance Control Dynam* **13**, 57-65(1990).

24. R. C. Thompson, J. L. Junkins and S. R. Vadali, Near-Minimum-Time Open-Loop Slewing of Flexible Vehicles. *J. Guidance Control Dynam* **13**, 82-88(1989).

25. R. D. Quinn and L. Meirovitch, Maneuvering and Vibration Control of SCOLE. *J. Guidance Control Dynam* **11**, 542-553(1988).

26. J. L. Junkins and H. Bang, Maneuver and Vibration Control of Hybrid Coordinate Systems using Lyapunov Stability Theory. *J. Guidance Control Dynam* **16**, 665-676(1993).

27. J. L. Junkins, Z. Rahman and H. Bang, Near Minimum-Time Maneuvers of Flexible Vehicles: Analytical and Experimental Results. *J. Guidance Control Dynam* **14**, 406-415(1991).

28. S. N. Singh, Robust Nonlinear Atitude Control of Flexible Spacecraft. *IEEE Transactions on Aerospace and Electronic Systems* **23**, 380-387(1987).

29. S. N. Singh, Flexible Spacecraft Maneuver-Inverse Attitude Control and Modal Stabilization. *Acta Astronautica* **17**, 1-9(1988).

30. S. N. Singh, Nonlinear Attitude Control of Flexible Spacecraft Under Disturbance Torque. *Acta Astronautica* **13**, 507-514(1986).

31. H. Oz and U.Ozguner, Variable Structure System Control of Flexible Spacecraft. *AIAA*, 84-2002(1984).

32. A. Iyer and S. N. Singh, Variable Structure Slewing Control and Vibration Damping of Flexible Spacecraft. *Acta Astronautica* **25**, 1-9(1991).

33. D. C. Hyland, J. L. Junkins and R. W. Longman, Active Control Technology for Space Structures. *J. Guidance Control Dynam* **16**, 801-821(1993).

34. P. V. Kokotovic, H. K. Khalil and J. O'Reilly, *Singular Perturbation Methods in Control : Analysis and Design,* Academic Press, New York, 1986.

35. H. K. Khalil, *Nonlinear Systems*, Macmillan Publishing Company, New York, 1992.

36. M. Suzuki, Composite Controls for Singularly Perturbed Systems, *IEEE Transactions on Automatic Control*, Vol. AC-26, pp.505-507, 1981.

37. D. S. Naidu, *Singular Perturbation Methodology in Control Systems*, Peter Peregrinus, London, 1988.

38. B. Siciliano and W. J. Book, A Singular Perturbation Approach to Control of Lightweight Flexible Manipulators. *The International Journal of Robotics Research*, Vol.7 No.4, pp.79-90, 1988.

39. F. L. Lewis and M. Vandegrift, Flexible Robot Arm Control by a Feedback Linearization/Singular Perturbation Approach, *Proceedings of American Control Conference*, San Francisco, June 1993, pp.729-736.

40. J. Storch and S. Gates, Planar Dynamics of a uniform beam with rigid bodies affixed to the ends. Technical Report CSDL-R-1629, The Charles Stark Draper Laboratory, Cambridge, Mass.(1983).

41. M. Athans, and P. L. Falb, *Optimal Control*, McGraw-Hill, New York, 1966.